

Singly Cabibbo-suppressed hadronic weak decays of the Ω^- hyperon

Ye Cao,^{1,*} Tao Zhong,^{2,†} Ju-Jun Xie,^{1,3,4,‡} and Qiang Zhao^{5,6,7,§}

¹*Southern Center for Nuclear-Science Theory (SCNT),
Institute of Modern Physics, Chinese Academy of Sciences, Huizhou 516000, China*

²*School of Physics and Mechatronic Engineering,
Guizhou Minzu University, Guiyang 550025, China*

³*Heavy Ion Science and Technology Key Laboratory, Institute of Modern Physics,
Chinese Academy of Sciences, Lanzhou 730000, China*

⁴*School of Nuclear Sciences and Technology, University of Chinese Academy of Sciences, Beijing 101408, China*

⁵*Institute of High Energy Physics, Chinese Academy of Sciences, Beijing 100049, China*

⁶*University of Chinese Academy of Sciences, Beijing 100049, China*

⁷*Center for High Energy Physics, Henan Academy of Sciences, Zhengzhou 450046, China*

We study the two-body hadronic weak decays of the Ω^- hyperon with strangeness $S = -3$, including three singly Cabibbo-suppressed decay modes: $\Xi^0\pi^-$, $\Xi^-\pi^0$ and ΛK^- . The decay amplitudes at the quark level, arising from $s \rightarrow ud\bar{u}$ transitions (direct pion emission and color-suppressed processes) and $su \rightarrow ud$ transitions (pole terms), are calculated in the framework of the non-relativistic constituent quark model. The theoretical results show that the $\Xi^0\pi^-$ channel is dominated by the color-allowed direct pion emission process, while the ΛK^- channel is well described by one type of pole contribution mediated through intermediate Ξ resonances ($1^2S_{1/2+}$ and $1^2P_{1/2-}$ states). However, the contribution from tree-level mechanisms alone to the branching ratio of $\Omega^- \rightarrow \Xi^-\pi^0$ is small due to its color-suppressed nature. The discrepancy is resolved by including final state interactions through rescattering processes via intermediate states $\Xi^0\pi^-$ and ΛK^- . This work demonstrates that a unified description of Ω^- hadronic weak decays necessitates the interplay of quark-level weak vertices, baryon pole structures, and long-distance final state rescattering dynamics. With these mechanisms, the obtained branching ratios are in agreement with the high-precision experimental data from the BESIII. Furthermore, these above decays are found to be dominated by the parity-conserving P -wave transitions, thus the asymmetry parameters are almost zero.

PACS numbers:

Keywords:

I. INTRODUCTION

Although the Ω^- hyperon with strangeness $S = -3$ was discovered 60 years ago [1], its spin was not experimentally determined until 2006 [2]. And many of its decay modes are still poorly known experimentally [3]. The Ω^- occupies a special role in the lowest-lying spin-3/2 decuplet of flavor SU(3) symmetry. All other decuplet states are dominated by the strong decay modes, however, the Ω^- decays only via the weak interaction. Its primary decay channels, as measured with high precision by the BESIII collaboration, are $\Omega^- \rightarrow \Lambda K^-$ with a branching ratio of $(66.3 \pm 0.8 \pm 2.0)\%$, and decays involving a Ξ hyperon, such as $\Omega^- \rightarrow \Xi^0\pi^-$ with a branching ratio of $(25.03 \pm 0.44 \pm 0.53)\%$, and $\Omega^- \rightarrow \Xi^-\pi^0$

of $(8.43 \pm 0.52 \pm 0.28)\%$ [4]. Moreover, the first model-independent determination of the Ω^- spin was conducted to be 3/2 by the BESIII collaboration in 2021 [5] since its discovery more than 50 years ago, and the decay parameters of the process $\Omega^- \rightarrow \Lambda K^-$ ($\bar{\Omega}^+ \rightarrow \bar{\Lambda}K^+$) were measured for the first time by a fit to the angular distribution of the complete decay chain.

The nonleptonic decay amplitudes of the Ω^- have been predominantly calculated within the framework of chiral perturbation theory (ChPT), the effective field theory of quantum chromodynamics (QCD) at low energies. A systematic analysis was studied by Ref. [6], which treated baryons as heavy particles in a low-energy chiral Lagrangian. This work found that the three dominant Ω^- decay modes proceed via P -wave and are governed by a single pole diagram at leading order. The heavy baryon ChPT was extended to the one-loop level in Ref. [7], incorporating the leading nonanalytic corrections. The role of intermediate resonances was further examined by the work of Ref. [8], suggesting that $J^P = \frac{1}{2}^\pm$ resonances play an essential role in these hadronic weak decays of Ω^- . In addition, Ref. [9] provided estimates of the branch-

*Electronic address: caoye@impcas.ac.cn

†Electronic address: zhongtao@gzmu.edu.cn

‡Electronic address: xiejujun@impcas.ac.cn

§Electronic address: zhaoq@ihep.ac.cn

ing ratios by means of the QCD enhanced effective weak Hamiltonian supplemented by the SU(3) Skyrme model. Earlier work by Ref. [10] calculated the branching ratios using the Weinberg-Salam model with QCD corrections and the MIT bag model. These theoretical efforts have established a tentative and somewhat rough but still evolving picture of Ω^- decays, where precise predictions for all decay parameters remain challenging and highlight the critical need for precise experimental constraints.

The main purpose of this work is to systematically investigate the hadronic weak decays for $\Omega^- \rightarrow \Xi^0\pi^-$, $\Xi^-\pi^0$ and ΛK^- modes within a phenomenological framework. This analysis is motivated by the availability of new, high-precision experimental data [4], which calls for a renewed and more detailed theoretical examination. We employ a similar model that has been previously applied to describe the hadronic weak decays of the ordinary octet hyperons, such as Λ and Σ^\pm [11]. In these hadronic weak decays, the two-body final states can carry orbital angular momentum $L = 1$ (P -wave) for parity-conserving (PC) transition or $L = 2$ (D -wave) for parity-violating (PV) transition. By calculating the branching ratios and the asymmetry parameters for the Ω^- decays, we aim to provide predictions that can be directly compared with existing and forthcoming measurements. We anticipate that the results of this study will contribute significantly to a deeper understanding of the decay dynamics and polarization properties of spin-3/2 hyperons, offering insights into the weak interaction in the strange baryon sector.

As follows, we will first introduce the quark-level mechanism including $s \rightarrow u d \bar{u}$ and $s u \rightarrow u d$ processes and hadron-level final state interaction mechanism in Sec. II and Sec. III, respectively. Then, the calculation results for the partial widths and asymmetry parameters and discussions will be presented in Sec. V. A brief summary will be given in Sec. VI.

II. THE QUARK-LEVEL AMPLITUDES AND PHYSICAL OBSERVABLES

The corresponding transition diagrams at the quark level for these $\Omega^- \rightarrow \Xi^0\pi^-$, $\Xi^-\pi^0$, and ΛK^- decays are shown in Fig. 1. Among them, we find that the $\Xi^0\pi^-$ and $\Xi^-\pi^0$ channels proceed only via the direct pion emission (DPE) process and the color suppressed (CS) process respectively, while the ΛK^- channel involves both the color suppressed (CS) process and the pole term (PT) process. The DPE and CS processes share a common quark-level transition mechanism of $s \rightarrow u d \bar{u}$. They are distinguished by whether the W boson is emitted externally or internally, thereby a color suppression factor will be present in the CS amplitudes. With the s quark in the initial-state baryon converting to a u quark by emitting a W^- boson, the quark pair $d \bar{u}$ coupled to the W^- will directly hadronize into the final-state meson π^- for DPE process. In contrast, the CS process describes

the hadronization of the final-state meson with a quark in the initial-state baryon combined with the antiquark created by the W emission. Depending on how the antiquark from the W emission is combined with one quark from the initial baryon, the CS process can be categorized into two types: CS-1 and CS-2, as labeled in Fig. 1 for Ω decays. PT processes are driven by the quark-level $s u \rightarrow u d$ internal conversion, with the final-state meson emitted via strong interaction vertices, as illustrated in Fig. 1 (d). In such a transition the weak and strong interactions occur non-locally, and pole structures in the transition amplitudes can be identified. Typically, pole terms are two-step processes, where the weak transition either precedes or follows the strong meson emission, as noted in Ref. [11]. In this work, however, we find that only one sequence contributes to the ΛK^- channel: the weak interaction occurs first, followed by the strong interaction. This indicates that the pole-term mechanism in Ω^- decays may differ from those described in Refs. [11, 12].

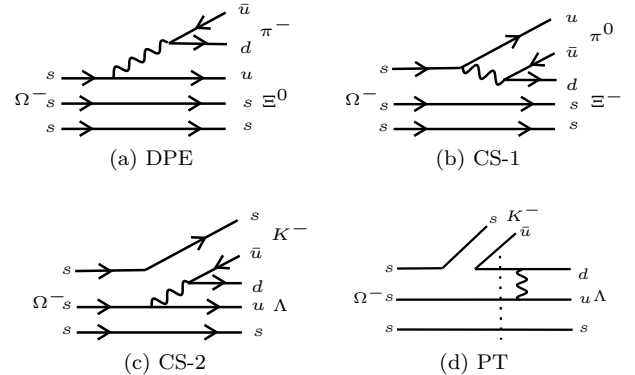


FIG. 1: Illustrations for the two-body hadronic weak decay of Ω^- into $\Xi\pi$ and ΛK^- at the quark level. (a) Direct pion emission (DPE) processes; (b)-(c) Color suppressed (CS) pion emission processes; (d) Pole terms (PT).

In the low energy regime, the constituent degrees of freedom become crucial, leading us to adopt the non-relativistic constituent quark model (NRCQM) to describe the baryon states in the transition amplitudes, which are expressed through wave function convolutions. The quark-level operators and wave functions will reveal some of the dynamical details of the interactions. The spin and flavor wave functions are trivial and listed in Appendix A, while the spatial wave functions can be obtained by numerically solving the Schrödinger equation for the baryon state, as presented in Sec. II C. Importantly, different transition amplitudes can be connected to each other through the SU(3) flavor symmetry. An interesting and non-negligible feature is that the SU(3) flavor symmetry should be broken and the breaking effects can be accounted for via both constituent quark mass and the wave function convolutions. This feature is different from hadron-level parametrization approaches, where the SU(3) flavor symmetry effects are absorbed into the coupling constants, leaving the connections and

relative phases among different transition amplitudes actually unclear. Therefore, in this section, we mainly introduce how to obtain the transition amplitude shown in Fig. 1 within the theoretical framework of NRCQM.

A. The decay amplitudes of $s \rightarrow ud\bar{u}$ processes

Within the NRCQM framework, transition amplitudes for both DPE and CS processes can be explicitly calcu-

lated without introducing additional parameters, since they are governed by the same quark-level operator $s \rightarrow ud\bar{u}$. It is generally assumed that the hadronic weak decay can be described by a current-current type Hamiltonian. In the non-relativistic limit, the effective weak Hamiltonian $\hat{H}_{W,1 \rightarrow 3}^{(\text{PC})}$ and $\hat{H}_{W,1 \rightarrow 3}^{(\text{PV})}$ for the $s_3 \rightarrow u_3 d_5 \bar{u}_4$ processes are written as:

$$\hat{H}_{W,1 \rightarrow 3}^{(\text{PC})} = \frac{G_F}{\sqrt{2}} \frac{\beta V_{ud} V_{us}}{(2\pi)^3} \hat{\alpha}_3^{(+)} \hat{I}_P \delta^3(\mathbf{p}_3 - \mathbf{p}'_3 - \mathbf{p}_4 - \mathbf{p}_5) \left\{ \left[\langle s'_3 | I | s_3 \rangle \langle s_5 \bar{s}_4 | \boldsymbol{\sigma} | 0 \rangle - \langle s'_3 | \boldsymbol{\sigma} | s_3 \rangle \langle s_5 \bar{s}_4 | I | 0 \rangle \right] \cdot \left[\left(\frac{\mathbf{p}_5}{2m_5} + \frac{\mathbf{p}_4}{2m_4} \right) - \left(\frac{\mathbf{p}'_3}{2m'_3} + \frac{\mathbf{p}_3}{2m_3} \right) \right] + i \langle s'_3 | \boldsymbol{\sigma} | s_3 \rangle \langle s_5 \bar{s}_4 | \boldsymbol{\sigma} | 0 \rangle \cdot \left[\left(\frac{\mathbf{p}_4}{2m_4} - \frac{\mathbf{p}_5}{2m_5} \right) - \left(\frac{\mathbf{p}_3}{2m_3} - \frac{\mathbf{p}'_3}{2m'_3} \right) \right] \right\}, \quad (1)$$

$$\hat{H}_{W,1 \rightarrow 3}^{(\text{PV})} = \frac{G_F}{\sqrt{2}} V_{ud} V_{us} \frac{\beta}{(2\pi)^3} \hat{\alpha}_3^{(+)} \hat{I}_P \delta^3(\mathbf{p}_3 - \mathbf{p}'_3 - \mathbf{p}_4 - \mathbf{p}_5) \left(-\langle s'_3 | I | s_3 \rangle \langle s_5 \bar{s}_4 | I | 0 \rangle + \langle s'_3 | \boldsymbol{\sigma} | s_3 \rangle \cdot \langle s_5 \bar{s}_4 | \boldsymbol{\sigma} | 0 \rangle \right), \quad (2)$$

where the superscript PC (PV) stands for the parity-conserving (parity-violating) operator. The Pauli operator $\boldsymbol{\sigma}$ and the momentum \mathbf{p}_i are the spin operator and spatial operator acting on the spin wave function and spatial wave function, respectively. $\hat{\alpha}^{(+)}$ is the flavor-changing operator that converts an s quark to a u quark, and \hat{I}_P is the isospin operator for the pseudoscalar meson (π and K) production process. It has the form of

$$\hat{I}_P^j = \begin{cases} b_{d,j}^\dagger b_{s,j} & \text{for } K^-, \\ \frac{1}{\sqrt{2}} b_{d,j}^\dagger b_{u,j} & \text{for } \pi^0, \end{cases} \quad (3)$$

for the singly Cabibbo-suppressed processes and will act on the j -th quark of the initial baryon after considering the flavor wave function of the emitted π and K . Combining the effects of flavor changing and π and K production, the flavor operator for the $\Omega^- \rightarrow \Xi^0 \pi^-, \Xi^- \pi^0$, and ΛK^- processes can be expressed as

$$\hat{O}_{\text{flavor}} = \begin{cases} b_{u,3}^\dagger b_{s,3} & \Omega^- \rightarrow \Xi^0 \pi^- \text{ [DE]}, \\ (b_{u,3}^\dagger b_{s,3})(\frac{1}{\sqrt{2}} b_{d,3}^\dagger b_{u,3}) & \Omega^- \rightarrow \Xi^- \pi^0 \text{ [CS-1]}, \\ (b_{u,3}^\dagger b_{s,3})(b_{d,1}^\dagger b_{s,1}) & \Omega^- \rightarrow \Lambda K^- \text{ [CS-2]}. \end{cases}$$

Since the $SU(6) \otimes O(3)$ wave functions of baryons are fully symmetric in flavor, spin, and space under interchange of any two quarks, thus we have

$$\langle \mathbb{B}_f | \sum_j \hat{H}_{W,s_j \rightarrow u_j d_5 \bar{u}_4}^{(\text{P})} | \mathbb{B}_i \rangle = \beta \langle \mathbb{B}_f | \hat{H}_{W,s_3 \rightarrow u_3 \bar{u}_4 d_5}^{(\text{P})} | \mathbb{B}_i \rangle, \quad (4)$$

where β is a symmetry factor and it takes a value of $A_3^1 = 3$ in the DPE and CS-1 processes, since in these two processes, there are two s quarks in Ω are the spectator quarks, while $A_3^2 = 6$ in the CS-2 processes since only one

s quark in Ω is the spectator quark. In addition, both the CS-1 and CS-2 processes include a color suppression factor of $1/3$.

Then, the transition amplitudes of the DPE and CS processes shown in Fig. 1 can be expressed as

$$\begin{aligned} \mathcal{M}_{\text{DPE/CS}}^{J_f, J_f^z; J_i, J_i^z} &= \langle \mathbb{B}_f(\mathbf{P}_f, J_f, J_f^z) \mathbb{M}(\mathbf{k}) | H_{W,1 \rightarrow 3}^{(\text{P})} | \mathbb{B}_i(\mathbf{P}_i, J_i, J_i^z) \rangle \\ &= \sum_{S_f^z, L_f^z; S_i^z, L_i^z} \langle \phi_f | \hat{\mathcal{O}}_{\text{flavor}} | \phi_i \rangle \langle \chi_{S_f, S_f^z} | \hat{\mathcal{O}}_{\text{spin}} | \chi_{S_i, S_i^z} \rangle \\ &\quad \times \langle \psi_P(\mathbf{k}) \psi_{N_f L_f L_f^z}(\mathbf{P}_f) | \hat{\mathcal{O}}_{\text{spatial}}(\mathbf{p}_i) | \psi_{N_i L_i L_i^z}(\mathbf{P}_i) \rangle \\ &= \sum_{S_f^z, L_f^z; S_i^z, L_i^z} \langle \phi_f | \hat{\mathcal{O}}_{\text{flavor}} | \phi_i \rangle \langle \chi_{S_f, S_f^z} | \hat{\mathcal{O}}_{\text{spin}} | \chi_{S_i, S_i^z} \rangle \\ &\quad \times I_{\text{DPE/CS}}^{L_f, L_f^z; L_i, L_i^z}. \end{aligned} \quad (5)$$

Apart from the color factor, the quark arrangements in the DPE and CS make a difference between these two processes via the spatial integrals. For the DPE process, the momentum conservation requires $\mathbf{P}_f = \mathbf{p}_1 + \mathbf{p}_2 + \mathbf{p}'_3$ and $\mathbf{k} = \mathbf{p}_5 + \mathbf{p}_4$, while $\mathbf{P}_f = \mathbf{p}_1 + \mathbf{p}_2 + \mathbf{p}_5$ and $\mathbf{k} = \mathbf{p}'_3 + \mathbf{p}_4$ for the CS-1 process; $\mathbf{P}_f = \mathbf{p}_5 + \mathbf{p}_2 + \mathbf{p}'_3$ and $\mathbf{k} = \mathbf{p}_1 + \mathbf{p}_4$ for the CS-2 process. They are guaranteed by the delta function in the following expressions of the spatial wave function convolution $I_{\text{DPE/CS}}^{L_f, L_f^z; L_i, L_i^z}$.

The flavor and spin matrix elements in Eq. (5) have different results for the DPE and CS processes. They are listed separately in Tabs. I and II. The spatial matrix elements can be described by the overlap integral of the initial-state wave function acting under the spatial operator with the final-state wave function. Taking the CS-1 process as an example, the expression is given by:

$$I_{\text{CS-1}}^{L_f, L_f^z; L_i, L_i^z} = \langle \psi_P(\mathbf{k}) \psi_{N_f L_f L_f^z}(\mathbf{P}_f) | \hat{\mathcal{O}}_{W,1 \rightarrow 3}^{\text{spatial}}(\mathbf{p}_i) | \psi_{N_i L_i L_i^z}(\mathbf{P}_i) \rangle = \int d\mathbf{p}_1 d\mathbf{p}_2 d\mathbf{p}_3 d\mathbf{p}'_1 d\mathbf{p}'_2 d\mathbf{p}'_3 d\mathbf{p}_4 d\mathbf{p}_5 \times \psi_P^*(\mathbf{p}'_3, \mathbf{p}_4) \delta^3(\mathbf{p}'_1 - \mathbf{p}_1) \delta^3(\mathbf{p}'_2 - \mathbf{p}_2) \delta^3(\mathbf{p}_3 - \mathbf{p}'_3 - \mathbf{p}_4 - \mathbf{p}_5) \psi_{N_f L_f L_f^z}^*(\mathbf{p}_1, \mathbf{p}_2, \mathbf{p}_5) \psi_P^*(\mathbf{p}'_3, \mathbf{p}_4) \times \hat{\mathcal{O}}_{W,1 \rightarrow 3}^{\text{spatial}}(\mathbf{p}_i) \psi_{N_i L_i L_i^z}(\mathbf{p}_1, \mathbf{p}_2, \mathbf{p}_3) \delta^3(\mathbf{P}_i - \mathbf{p}_1 - \mathbf{p}_2 - \mathbf{p}_3) \delta^3(\mathbf{k} - \mathbf{p}'_3 - \mathbf{p}_4) \delta^3(\mathbf{P}_f - \mathbf{p}'_1 - \mathbf{p}'_2 - \mathbf{p}_5), \quad (6)$$

where $\hat{\mathcal{O}}_{W,1 \rightarrow 3}^{\text{spatial}}(\mathbf{p}_i)$ is a function of the quark momentum \mathbf{p}_i , such as $\mathbf{p}_5/(2m_5) + \mathbf{p}_4/(2m_4)$ or just 1 for $H_{W,1 \rightarrow 3}^{(\text{PV})}$. The significant difference between the two integral functions $I_{\text{DPE}}^{L_f, L_f^z; L_i, L_i^z}$ and $I_{\text{CS}}^{L_f, L_f^z; L_i, L_i^z}$ is the different momentum conservation conditions. It indicates that, for the DPE and CS processes, apart from the color suppression factor of 1/3, there are also differences in the convolution of their spatial wave functions. This is a dynamic feature with the quark model approach.

TABLE I: The flavor matrix elements in the DPE and CS processes for Ω^- decays.

Decay channels	Processes	$\langle \phi_f^\lambda \hat{\mathcal{O}}_{\text{flavor}} \phi_i^s \rangle$	$\langle \phi_f^\rho \hat{\mathcal{O}}_{\text{flavor}} \phi_i^s \rangle$
$\Omega^- \rightarrow \Xi^0 \pi^-$	DPE	$\frac{2}{\sqrt{6}}$	0
$\Omega^- \rightarrow \Xi^- \pi^0$	CS-1	$\frac{1}{\sqrt{3}}$	0
$\Omega^- \rightarrow \Lambda K^-$	CS-2	$-\frac{1}{2}$	$-\frac{1}{2\sqrt{3}}$

TABLE II: The spin matrix elements for the PC and PV transitions in the DPE and CS processes.

$\mathcal{O}_{\text{spin}}^{(\text{PC})}$	$\langle \chi_{\frac{1}{2}, -\frac{1}{2}}^\lambda \mathcal{O}_{\text{spin}}^{(\text{PC})} \chi_{\frac{3}{2}, -\frac{1}{2}}^s \rangle$			$\langle \chi_{\frac{1}{2}, -\frac{1}{2}}^\rho \mathcal{O}_{\text{spin}}^{(\text{PC})} \chi_{\frac{3}{2}, -\frac{1}{2}}^s \rangle$		
	DPE	CS-1	CS-2	DPE	CS-1	CS-2
$\langle s'_3 I s_3 \rangle \langle s_5 \bar{s}_4 \sigma 0 \rangle$	0	$\frac{2}{3} \hat{\mathbf{k}}$	$-\frac{1}{3} \hat{\mathbf{k}}$	0	0	$-\frac{1}{\sqrt{3}} \hat{\mathbf{k}}$
$\langle s'_3 \sigma s_3 \rangle \langle s_5 \bar{s}_4 I 0 \rangle$	$\frac{4}{3} \hat{\mathbf{k}}$	$\frac{2}{3} \hat{\mathbf{k}}$	$\frac{2}{3} \hat{\mathbf{k}}$	0	0	0
$\langle s'_3 \sigma s_3 \rangle \langle s_5 \bar{s}_4 \sigma 0 \rangle$	0	$-\frac{4}{3} i \hat{\mathbf{k}}$	$i \hat{\mathbf{k}}$	0	0	$\frac{1}{\sqrt{3}} i \hat{\mathbf{k}}$
$\mathcal{O}_{\text{spin}}^{(\text{PV})}$	$\langle \chi_{\frac{1}{2}, -\frac{1}{2}}^\lambda \mathcal{O}_{\text{spin}}^{(\text{PV})} \chi_{\frac{3}{2}, -\frac{1}{2}}^s \rangle$			$\langle \chi_{\frac{1}{2}, -\frac{1}{2}}^\rho \mathcal{O}_{\text{spin}}^{(\text{PV})} \chi_{\frac{3}{2}, -\frac{1}{2}}^s \rangle$		
	DPE	CS-1	CS-2	DPE	CS-1	CS-2
$\langle s'_3 I s_3 \rangle \langle s_5 \bar{s}_4 I 0 \rangle$	0	0	0	0	0	0
$\langle s'_3 \sigma s_3 \rangle \cdot \langle s_5 \bar{s}_4 \sigma 0 \rangle$	0	0	0	0	0	0

We now focus on the $\Xi^0 \pi^-$ and $\Xi^- \pi^0$ decay modes. Neglecting differences from final-state hadronization (i.e., the convolution of wave functions), the DPE amplitude for $\Omega^- \rightarrow \Xi^0 \pi^-$ and the CS amplitude for $\Omega^- \rightarrow \Xi^- \pi^0$ (see Fig. 1) satisfy the relation

$$\frac{\mathcal{M}_{\text{CS}}(\Omega^- \rightarrow \Xi^- \pi^0)}{\mathcal{M}_{\text{DPE}}(\Omega^- \rightarrow \Xi^0 \pi^-)} = -\frac{1}{3\sqrt{2}}, \quad (7)$$

where $1/3$ and $-1/\sqrt{2}$ are respectively the color suppression factor and the isospin factor of π^0 . Then taking into account the phase spaces for these two channels are nearly identical, the relation of the decay branching ratios (BR) contributed by the $s \rightarrow u \bar{d} \bar{u}$ weak transitions for these two channels is $BR_{\text{DPE}}(\Omega^- \rightarrow \Xi^0 \pi^-) \simeq 18 \times BR_{\text{CS}}(\Omega^- \rightarrow \Xi^- \pi^0)$. This ratio is seriously inconsistent with the experimental value of $BR_{\text{exp}}(\Omega^- \rightarrow \Xi^0 \pi^-) \simeq 3 \times BR_{\text{exp}}(\Omega^- \rightarrow \Xi^- \pi^0)$ that was measured by BESIII Collaboration [4].

We next focus on the $\Xi^0 \pi^-$ and ΛK^- decay modes. As seen in Figs. 1 (a) and (c), the DPE amplitude for $\Xi^0 \pi^-$ is larger than the CS amplitude for ΛK^- . This implies that, considering only the $s \rightarrow u \bar{d} \bar{u}$ weak transition contributions, the $\Xi^0 \pi^-$ channel should have a higher branching ratio than the ΛK^- channel. However, this implication is also inconsistent with experimental data, which show that $\Omega^- \rightarrow \Lambda K^-$ has the largest branching ratio among these decay modes [4].

From the preceding qualitative analysis above, we find that the $s \rightarrow u \bar{d} \bar{u}$ transition is insufficient to explain the dynamical mechanisms of the hadronic weak decays of the Ω hyperon. A complete description must incorporate other underlying mechanisms, which are inherently related to the non-perturbative strong-interaction dynamics.

B. The decay amplitudes of $su \rightarrow ud$ processes

The hyperon two-body hadronic weak decays also involve a typical transition processes known as the pole terms which describe the $su \rightarrow ud$ internal conversion mechanism via W -boson exchange. As shown in Fig. 1, in Ω decays, only the ΛK^- channel contains such a pole process where the strong interaction that emits a kaon meson first occurs, followed by the weak interaction that changes the flavor. For the pole terms, the general expression of decay amplitude can be written as

$$\mathcal{M}_{\text{PT(PC)}}^{J_f, J_f^z; J_i, J_i^z} = \sum_{\mathbb{B}_m} \langle \mathbb{B}_f(\mathbf{P}_f; J_f, J_f^z) | \frac{i\hat{H}_{W,2 \rightarrow 2}^{(\text{PC})}}{\not{p}_{\mathbb{B}_m} - m_{\mathbb{B}_m} + i\frac{\Gamma_{\mathbb{B}_m}}{2}} | \mathbb{B}_m(\mathbf{P}_f; J_f, J_f^z) \rangle \langle \mathbb{B}_m(\mathbf{P}_f; J_f, J_f^z) | \hat{H}_P | \mathbb{B}_i(\mathbf{P}_i; J_i, J_i^z) \rangle, \quad (8)$$

$$\mathcal{M}_{\text{PT(PV)}}^{J_f, J_f^z; J_i, J_i^z} = \sum_{\mathbb{B}'_m} \langle \mathbb{B}_f(\mathbf{P}_f; J_f, J_f^z) | \frac{i\hat{H}_{W,2 \rightarrow 2}^{(\text{PV})}}{\not{p}_{\mathbb{B}'_m} - m_{\mathbb{B}'_m} + i\frac{\Gamma_{\mathbb{B}'_m}}{2}} | \mathbb{B}'_m(\mathbf{P}_f; J_f, J_f^z) \rangle \langle \mathbb{B}'_m(\mathbf{P}_f; J_f, J_f^z) | \hat{H}_P | \mathbb{B}_i(\mathbf{P}_i; J_i, J_i^z) \rangle, \quad (9)$$

where \mathbb{B}_m and \mathbb{B}'_m denote the intermediate baryon states with quantum numbers of $J^P = \frac{1}{2}^+$ and $\frac{1}{2}^-$, respectively. The dominant contributions of the pole terms come from the processes that the intermediate states are approximately on-shell. In our calculation, the approximation of propagator

$$\frac{1}{\not{p} - m + i\Gamma/2} \approx \frac{2m}{p^2 - m^2 + im\Gamma}. \quad (10)$$

is applied. It should be noted that this treatment will bring uncertainties into the theoretical results since the intermediate states are generally off-shell. Nevertheless, such uncertainties can be absorbed into the quark model parameters for which the range of the favored values by experimental data can be estimated.

In this work, the intermediate state is identified as the Ξ resonance with the flavor component *uss*. There are only two Ξ baryons with 4-star ratings whose spin and parity are known, as reported in the most recent PDG listings [3]. They are the octet ground states $\Xi(1315)^0$ and $\Xi(1322)^-$ with $J^P = \frac{1}{2}^+$ ($1^2S_{\frac{1}{2}+}$), and the decuplet ground state $\Xi(1535)$ with $J^P = \frac{3}{2}^+$ ($1^4S_{\frac{3}{2}+}$). However, the low-lying excitation states with negative parity, i.e., $\Xi(\frac{1}{2}^-)$ have not been determined experimentally. There are two candidates listed in the PDG, one is the 2-star state $\Xi(1620)$ with mass about 1620 MeV and width of 32^{+8}_{-9} MeV, and the other one is 3-star state $\Xi(1690)$ with mass of 1690 ± 10 MeV and width of 20 ± 15 MeV. The higher-mass state made its debut in 1980 as $\Xi(1680)S_{11}$. The BaBar collaboration, in their analysis of the decay $\Lambda_c^+ \rightarrow \Xi^-\pi^+K^+$ and quantitative description of the $\Xi(1530)^0$ line shape, determined the J^P quantum numbers of the $\Xi(1690)^0$ to be $\frac{1}{2}^-$ [13]. Furthermore, the BESIII collaboration, in a study of $\psi(3686)$ decays, observed the $\Xi(1690)^-$ in the $K^-\Lambda$ spectrum and confirmed its J^P as $\frac{1}{2}^-$ through a partial wave analysis [14]. This J^P assignment is consistent with that of BaBar, but the reported width of 81^{+10}_{-9} is larger. However the evidence for the lower-mass $\Xi(1620)$ has been rather weak until recently. On the theoretical front, quark-model studies offer predictions for $\Xi(\frac{1}{2}^-)$ states. Ref. [15] assigned the $\Xi(1690)$ to the first orbital excitation $1^2P_{\frac{1}{2}-}$, based on calculations of its partial decay widths in the chiral quark model and comparison with experimental data. Similarly, Pervin and Roberts proposed that $\Xi(1690)$ could be

identified as the first orbital excitation with $J^P = \frac{1}{2}^-$, although their model predicted a mass about 35 MeV heavier than the $\Xi(1690)$ [16]. They believed that a more microscopic treatment of spin-orbit interactions, can be expected to drive this state to slightly lower mass. Consequently, for the pole term processes, we adopt the following treatment: the nonfactorizable PV amplitude primarily arises from the first orbital excitation state $1^2P_{\frac{1}{2}-}$, while the nonfactorizable PC amplitude is determined by the ground state $1^2S_{\frac{1}{2}+}$.

The chiral quark model (CQM) has been often applied to the production of light pseudoscalar mesons in various processes [17, 18]. In this work, for the strong interaction vertex of the kaon emission that occurred first as shown in Fig. 1 (d), we employ the CQM to study it with the transition Hamiltonian given by:

$$\hat{H}_P = \frac{1}{f_P} \sum_j \bar{\psi}_j \gamma_\mu \gamma_5 \partial^\mu \phi_P \hat{I}_j^P \psi_j, \quad (11)$$

where f_P is the decay constant of the pseudoscalar meson, and j denotes the j -th quark inside the baryon that interacts with the emitted pseudoscalar meson. In momentum representation, the chiral Lagrangian for quark-pseudoscalar meson pseudovector coupling reduces to the non-relativistic form up to $1/m$ order as:

$$\hat{H}_P^{NR} = \frac{1}{f_P \sqrt{(2\pi)^3 2\omega}} \sum_j \left[\frac{\omega}{2m_j} \boldsymbol{\sigma}_j \cdot \mathbf{p}_j + \frac{\omega}{2m'_j} \boldsymbol{\sigma}_j \cdot \mathbf{p}'_j - \boldsymbol{\sigma}_j \cdot \mathbf{k} \right] \hat{I}_j^P \delta^3(\mathbf{p}_j - \mathbf{p}'_j - \mathbf{k}), \quad (12)$$

where ω and \mathbf{k} are the energy and three-momentum of the final-state pseudoscalar meson in the initial-state rest frame; \mathbf{p}_j and \mathbf{p}'_j are the three-momenta of the j -th quark before and after emitting the pseudoscalar meson. For the pole term contribution to the $\Omega^- \rightarrow \Lambda K^-$ decay, we take the kaon decay constant $f_K = 159$ MeV and $\hat{I}_j^{K^-} = a_j^\dagger(u) a_j(s)$ is the isospin operator for the K^- production shown in Fig. 1 with $a_j^\dagger(u)$ and $a_j(s)$ representing the creation and annihilation operators for quarks. This isospin operator acts on the flavor wave function, and the only non-vanishing flavor matrix elements is $\langle \phi_{\Xi^0}^\lambda | \hat{I}_3^{K^-} | \phi_{\Omega^-}^s \rangle = 2/\sqrt{6}$.

Since the baryon wave function is fully symmetric with the asymmetric color wavefunction, the strong interaction matrix element can be simplified using

$\langle \mathbb{B}_f | \sum_{j=1}^3 \hat{H}_{Pj}^{NR} | \mathbb{B}_i \rangle = 3 \langle \mathbb{B}_f | \hat{H}_{P(j=3)}^{NR} | \mathbb{B}_i \rangle$. The Pauli operator and momentum operator in Eq. (12) are coupled together, and we handle them by defining ladder operators,

$$\boldsymbol{\sigma}_j \cdot \mathbf{p}_j = \sigma_j^+ p_j^- + \sigma_j^- p_j^+ + \sigma_{jz} p_{jz}, \quad (13)$$

where

$$\begin{cases} \sigma_j^+ = \frac{1}{2}(\sigma_{jx} + i\sigma_{jy}), \\ \sigma_j^- = \frac{1}{2}(\sigma_{jx} - i\sigma_{jy}) \end{cases} \text{ and } \begin{cases} p_j^+ = p_{jx} + ip_{jy} \\ p_j^- = p_{jx} - ip_{jy} \end{cases}. \quad (14)$$

The Pauli operator acts on the spin wave function, and the non-vanishing spin matrix elements are $\langle \chi_{\frac{1}{2}, -\frac{1}{2}}^\lambda | \sigma_{3z} | \chi_{\frac{3}{2}, -\frac{1}{2}}^s \rangle = -\frac{4}{3\sqrt{2}}$ and $\langle \chi_{\frac{1}{2}, \frac{1}{2}}^\lambda | \sigma_3^+ | \chi_{\frac{3}{2}, -\frac{1}{2}}^s \rangle = -\frac{2}{3\sqrt{2}}$. Finally, for the strong matrix element in Eq. (9), we have

$$\begin{aligned} \langle \mathbb{B}_m(\mathbf{P}_f; J_f, J_f^z) | \hat{H}_P | \mathbb{B}_i(\mathbf{P}_i; J_i, J_i^z) \rangle &= \frac{3}{f_P \sqrt{(2\pi)^3 2\omega}} \sum_{S_f^z, L_f^z, S_i^z, L_i^z} \langle \phi_f | \hat{I}_3^P | \phi_i \rangle \langle \chi_{S_f, S_f^z} | \hat{\mathcal{O}}_{\text{spin}}(\sigma_{3z}, \sigma_3^+, \sigma_3^-) | \chi_{S_i, S_i^z} \rangle \\ &\times \int d\mathbf{p}_1 d\mathbf{p}_2 d\mathbf{p}_3 d\mathbf{p}'_1 d\mathbf{p}'_2 d\mathbf{p}'_3 \delta^3(\mathbf{p}'_1 - \mathbf{p}_1) \delta^3(\mathbf{p}'_2 - \mathbf{p}_2) \delta^3(\mathbf{p}'_3 - \mathbf{p}_3 + \mathbf{k}) \psi_{N_f L_f L_f^z}^*(\mathbf{p}'_1, \mathbf{p}'_2, \mathbf{p}'_3) \hat{\mathcal{O}}_P^{\text{spatial}}(\mathbf{p}_{3z}, \mathbf{p}_3^+, \mathbf{p}_3^-) \\ &\times \psi_{N_i L_i L_i^z}(\mathbf{p}_1, \mathbf{p}_2, \mathbf{p}_3) \delta^3(\mathbf{P}_i - \mathbf{p}_1 - \mathbf{p}_2 - \mathbf{p}_3) \delta^3(\mathbf{P}_f - \mathbf{p}'_1 - \mathbf{p}'_2 - \mathbf{p}'_3). \end{aligned} \quad (15)$$

Subsequently, for the $su \rightarrow ud$ internal conversion process as shown in Fig. 1 (d), the non-relativistic Hamiltonian can be written as

$$\begin{aligned} \hat{H}_{W,2 \rightarrow 2}^{(\text{PC})} &= \frac{G_F}{\sqrt{2}} \frac{V_{q_1 q'_1} V_{q_2 q'_2}}{(2\pi)^3} \sum_{i \neq j} \hat{\alpha}_i^{(-)} \hat{\beta}_j^{(+)} \times \\ &\delta^3(\mathbf{p}'_i + \mathbf{p}'_j - \mathbf{p}_i - \mathbf{p}_j) \left(\langle s_i' | I | s_i \rangle \langle s'_j | I | s_j \rangle - \langle s_i' | \boldsymbol{\sigma}_i | s_i \rangle \cdot \langle s'_j | \boldsymbol{\sigma}_j | s_j \rangle \right), \quad (16) \\ \hat{H}_{W,2 \rightarrow 2}^{(\text{PV})} &= \frac{G_F}{\sqrt{2}} \frac{V_{q_1 q'_1} V_{q_2 q'_2}}{(2\pi)^3} \sum_{i \neq j} \hat{\alpha}_i^{(-)} \hat{\beta}_j^{(+)} \times \\ &\delta^3(\mathbf{p}'_i + \mathbf{p}'_j - \mathbf{p}_i - \mathbf{p}_j) \left\{ \left(\langle s_i' | I | s_i \rangle \langle s'_j | \boldsymbol{\sigma}_j | s_j \rangle - \langle s_i' | \boldsymbol{\sigma}_i | s_i \rangle \langle s'_j | I | s_j \rangle \right) \cdot \left[\left(\frac{\mathbf{p}_i}{2m_i} - \frac{\mathbf{p}_j}{2m_j} \right) + \left(\frac{\mathbf{p}'_i}{2m'_i} - \frac{\mathbf{p}'_j}{2m'_j} \right) \right] \right. \\ &+ i \left(\langle s_i' | \boldsymbol{\sigma}_i | s_i \rangle \times \langle s'_j | \boldsymbol{\sigma}_j | s_j \rangle \right) \cdot \\ &\left. \left[\left(\frac{\mathbf{p}_i}{2m_i} - \frac{\mathbf{p}_j}{2m_j} \right) - \left(\frac{\mathbf{p}'_i}{2m'_i} - \frac{\mathbf{p}'_j}{2m'_j} \right) \right] \right\}, \quad (17) \end{aligned}$$

where the subscripts i and j ($i, j = 1, 2, 3$ and $i \neq j$) indicate the quarks experiencing the weak interaction; $\hat{\alpha}_i^{(-)}$ and $\hat{\beta}_j^{(+)}$ are the flavor-changing operators, namely, $\alpha_i^{(-)} u_j = \delta_{ij} d_i$, $\beta_j^{(+)} s_i = \delta_{ij} u_j$. In the calculation, we can fix the subscripts i and j to be 1 and 2 due to the symmetry of the total wave function, then the weak transition matrix element can be simplified to $\langle \mathbb{B}_f | \sum_{i \neq j} \hat{H}_{W,u_i s_j \rightarrow d_i u_j}^{(\text{P})} | \mathbb{B}_i \rangle = 3 \langle \mathbb{B}_f | \hat{H}_{W,u_1 s_2 \rightarrow d_1 u_2}^{(\text{P})} | \mathbb{B}_i \rangle$. Under this quark label, the non-vanishing flavor matrix elements are $\langle \phi_\Lambda^\rho | \hat{\alpha}_1^{(-)} \hat{\beta}_2^{(+)} | \phi_{\Xi^0}^\lambda \rangle = \frac{1}{3\sqrt{2}}$ and $\langle \phi_\Lambda^\rho | \hat{\alpha}_1^{(-)} \hat{\beta}_2^{(+)} | \phi_{\Xi^0}^\rho \rangle = \frac{1}{\sqrt{6}}$. All these include spin matrix elements are summarized in Tab. III.

Finally, the weak matrix element for PC transition can be obtained by producing the integration as

$$\begin{aligned} \langle \mathbb{B}_f(\mathbf{P}_f; J_f, J_f^z) | \hat{H}_{W,2 \rightarrow 2}^{(\text{PC})} | \mathbb{B}_m(\mathbf{P}_f; J_f, J_f^z) \rangle &= \frac{G_F}{\sqrt{2}} \frac{6V_{ud}V_{us}}{(2\pi)^3} \sum_{S_f^z, L_f^z, S_i^z, L_i^z} \langle \phi_f | \hat{\alpha}_1^{(-)} \hat{\beta}_2^{(+)} | \phi_i \rangle \langle \chi_{S_f, S_f^z} | 1 - \boldsymbol{\sigma}_1 \cdot \boldsymbol{\sigma}_2 | \chi_{S_i, S_i^z} \rangle \\ &\times \int d\mathbf{p}_1 d\mathbf{p}_2 d\mathbf{p}_3 \mathbf{p}'_1 \mathbf{p}'_2 \mathbf{p}'_3 \delta^3(\mathbf{p}'_1 + \mathbf{p}'_2 - \mathbf{p}_1 - \mathbf{p}_2) \delta^3(\mathbf{p}'_3 - \mathbf{p}_3) \psi_{N_f L_f L_f^z}^*(\mathbf{p}'_1, \mathbf{p}'_2, \mathbf{p}'_3) \psi_{N_i L_i L_i^z}(\mathbf{p}_1, \mathbf{p}_2, \mathbf{p}_3) \\ &\times \delta^3(\mathbf{P}_f - \mathbf{p}_1 - \mathbf{p}_2 - \mathbf{p}_3) \delta^3(\mathbf{P}_f - \mathbf{p}'_1 - \mathbf{p}'_2 - \mathbf{p}'_3). \end{aligned} \quad (18)$$

Analogously, we also can obtain the weak transition ma-

trix element $\langle \mathbb{B}_f(\mathbf{P}_f; J_f, J_f^z) | \hat{H}_{W,2 \rightarrow 2}^{(\text{PV})} | \mathbb{B}_m(\mathbf{P}_f; J_f, J_f^z) \rangle$.

TABLE III: The spin matrix elements for the PC and PV transitions in the weak internal conversion process.

$\mathcal{O}_{\text{spin}}^{(\text{PC})}$	$\langle \chi_{\frac{1}{2}, -\frac{1}{2}}^{\lambda} \mathcal{O}_{\text{spin}}^{(\text{PC})} \chi_{\frac{1}{2}, -\frac{1}{2}}^{\lambda} \rangle$	$\langle \chi_{\frac{1}{2}, -\frac{1}{2}}^{\lambda} \mathcal{O}_{\text{spin}}^{(\text{PC})} \chi_{\frac{1}{2}, -\frac{1}{2}}^{\rho} \rangle$	$\langle \chi_{\frac{1}{2}, -\frac{1}{2}}^{\rho} \mathcal{O}_{\text{spin}}^{(\text{PC})} \chi_{\frac{1}{2}, -\frac{1}{2}}^{\lambda} \rangle$	$\langle \chi_{\frac{1}{2}, -\frac{1}{2}}^{\rho} \mathcal{O}_{\text{spin}}^{(\text{PC})} \chi_{\frac{1}{2}, -\frac{1}{2}}^{\rho} \rangle$
$\langle s'_1 I s_1 \rangle \langle s'_2 I s_2 \rangle$	1	0	0	1
$\langle s'_1 \boldsymbol{\sigma} s_1 \rangle \cdot \langle s'_2 \boldsymbol{\sigma} s_2 \rangle$	1	0	0	-3
$I - \boldsymbol{\sigma}_1 \cdot \boldsymbol{\sigma}_2$	0	0	0	4
$\mathcal{O}_{\text{spin}}^{(\text{PV})}$	$\langle \chi_{\frac{1}{2}, -\frac{1}{2}}^{\lambda} \mathcal{O}_{\text{spin}}^{(\text{PV})} \chi_{\frac{1}{2}, -\frac{1}{2}}^{\lambda} \rangle$	$\langle \chi_{\frac{1}{2}, -\frac{1}{2}}^{\lambda} \mathcal{O}_{\text{spin}}^{(\text{PV})} \chi_{\frac{1}{2}, -\frac{1}{2}}^{\rho} \rangle$	$\langle \chi_{\frac{1}{2}, -\frac{1}{2}}^{\rho} \mathcal{O}_{\text{spin}}^{(\text{PV})} \chi_{\frac{1}{2}, -\frac{1}{2}}^{\lambda} \rangle$	$\langle \chi_{\frac{1}{2}, -\frac{1}{2}}^{\rho} \mathcal{O}_{\text{spin}}^{(\text{PV})} \chi_{\frac{1}{2}, -\frac{1}{2}}^{\rho} \rangle$
$\langle s'_1 I s_1 \rangle \langle s'_2 \boldsymbol{\sigma} s_2 \rangle$	$-\frac{2}{3} \hat{\mathbf{k}}$	$-\frac{1}{\sqrt{3}} \hat{\mathbf{k}}$	$-\frac{1}{\sqrt{3}} \hat{\mathbf{k}}$	0
$\langle s'_1 \boldsymbol{\sigma} s_1 \rangle \langle s'_2 I s_2 \rangle$	$-\frac{2}{3} \hat{\mathbf{k}}$	$\frac{1}{\sqrt{3}} \hat{\mathbf{k}}$	$\frac{1}{\sqrt{3}} \hat{\mathbf{k}}$	0
$\langle s'_1 \boldsymbol{\sigma} s_1 \rangle \times \langle s'_2 \boldsymbol{\sigma} s_2 \rangle$	0	$-\frac{2i}{\sqrt{3}} \hat{\mathbf{k}}$	$\frac{2i}{\sqrt{3}} \hat{\mathbf{k}}$	0
$I_1 \boldsymbol{\sigma}_2 - \boldsymbol{\sigma}_1 I_2$	0	$-\frac{2}{\sqrt{3}} \hat{\mathbf{k}}$	$-\frac{2}{\sqrt{3}} \hat{\mathbf{k}}$	0
$i \boldsymbol{\sigma}_1 \times \boldsymbol{\sigma}_2$	0	$\frac{2}{\sqrt{3}} \hat{\mathbf{k}}$	$-\frac{2}{\sqrt{3}} \hat{\mathbf{k}}$	0
$\mathcal{O}_{\text{spin}}^{(\text{PV})}$	$\langle \chi_{\frac{1}{2}, \frac{1}{2}}^{\lambda} \mathcal{O}_{\text{spin}}^{(\text{PV})} \chi_{\frac{1}{2}, -\frac{1}{2}}^{\lambda} \rangle$	$\langle \chi_{\frac{1}{2}, \frac{1}{2}}^{\lambda} \mathcal{O}_{\text{spin}}^{(\text{PV})} \chi_{\frac{1}{2}, -\frac{1}{2}}^{\rho} \rangle$	$\langle \chi_{\frac{1}{2}, \frac{1}{2}}^{\rho} \mathcal{O}_{\text{spin}}^{(\text{PV})} \chi_{\frac{1}{2}, -\frac{1}{2}}^{\lambda} \rangle$	$\langle \chi_{\frac{1}{2}, \frac{1}{2}}^{\rho} \mathcal{O}_{\text{spin}}^{(\text{PV})} \chi_{\frac{1}{2}, -\frac{1}{2}}^{\rho} \rangle$
$\langle s'_1 I s_1 \rangle \langle s'_2 \boldsymbol{\sigma} s_2 \rangle$	$\frac{2}{3} (\hat{\mathbf{i}} - i\hat{\mathbf{j}})$	$\frac{1}{\sqrt{3}} (\hat{\mathbf{i}} - i\hat{\mathbf{j}})$	$\frac{1}{\sqrt{3}} (\hat{\mathbf{i}} - i\hat{\mathbf{j}})$	0
$\langle s'_1 \boldsymbol{\sigma} s_1 \rangle \langle s'_2 I s_2 \rangle$	$\frac{2}{3} (\hat{\mathbf{i}} - i\hat{\mathbf{j}})$	$-\frac{1}{\sqrt{3}} (\hat{\mathbf{i}} - i\hat{\mathbf{j}})$	$-\frac{1}{\sqrt{3}} (\hat{\mathbf{i}} - i\hat{\mathbf{j}})$	0
$\langle s'_1 \boldsymbol{\sigma} s_1 \rangle \times \langle s'_2 \boldsymbol{\sigma} s_2 \rangle$	0	$\frac{2}{\sqrt{3}} (i\hat{\mathbf{i}} + \hat{\mathbf{j}})$	$-\frac{2}{\sqrt{3}} (i\hat{\mathbf{i}} + \hat{\mathbf{j}})$	0
$I_1 \boldsymbol{\sigma}_2 - \boldsymbol{\sigma}_1 I_2$	0	$\frac{2}{\sqrt{3}} (\hat{\mathbf{i}} - i\hat{\mathbf{j}})$	$\frac{2}{\sqrt{3}} (\hat{\mathbf{i}} - i\hat{\mathbf{j}})$	0
$i \boldsymbol{\sigma}_1 \times \boldsymbol{\sigma}_2$	0	$-\frac{2}{\sqrt{3}} (\hat{\mathbf{i}} - i\hat{\mathbf{j}})$	$\frac{2}{\sqrt{3}} (\hat{\mathbf{i}} - i\hat{\mathbf{j}})$	0
$\mathcal{O}_{\text{spin}}^{(\text{PV})}$	$\langle \chi_{\frac{1}{2}, -\frac{1}{2}}^{\lambda} \mathcal{O}_{\text{spin}}^{(\text{PV})} \chi_{\frac{1}{2}, \frac{1}{2}}^{\lambda} \rangle$	$\langle \chi_{\frac{1}{2}, -\frac{1}{2}}^{\lambda} \mathcal{O}_{\text{spin}}^{(\text{PV})} \chi_{\frac{1}{2}, \frac{1}{2}}^{\rho} \rangle$	$\langle \chi_{\frac{1}{2}, -\frac{1}{2}}^{\rho} \mathcal{O}_{\text{spin}}^{(\text{PV})} \chi_{\frac{1}{2}, \frac{1}{2}}^{\lambda} \rangle$	$\langle \chi_{\frac{1}{2}, -\frac{1}{2}}^{\rho} \mathcal{O}_{\text{spin}}^{(\text{PV})} \chi_{\frac{1}{2}, \frac{1}{2}}^{\rho} \rangle$
$\langle s'_1 I s_1 \rangle \langle s'_2 \boldsymbol{\sigma} s_2 \rangle$	$\frac{2}{3} (\hat{\mathbf{i}} + i\hat{\mathbf{j}})$	$\frac{1}{\sqrt{3}} (\hat{\mathbf{i}} + i\hat{\mathbf{j}})$	$\frac{1}{\sqrt{3}} (\hat{\mathbf{i}} + i\hat{\mathbf{j}})$	0
$\langle s'_1 \boldsymbol{\sigma} s_1 \rangle \langle s'_2 I s_2 \rangle$	$\frac{2}{3} (\hat{\mathbf{i}} + i\hat{\mathbf{j}})$	$-\frac{1}{\sqrt{3}} (\hat{\mathbf{i}} + i\hat{\mathbf{j}})$	$-\frac{1}{\sqrt{3}} (\hat{\mathbf{i}} + i\hat{\mathbf{j}})$	0
$\langle s'_1 \boldsymbol{\sigma} s_1 \rangle \times \langle s'_2 \boldsymbol{\sigma} s_2 \rangle$	0	$\frac{2}{\sqrt{3}} (i\hat{\mathbf{i}} - \hat{\mathbf{j}})$	$-\frac{2}{\sqrt{3}} (i\hat{\mathbf{i}} - \hat{\mathbf{j}})$	0
$I_1 \boldsymbol{\sigma}_2 - \boldsymbol{\sigma}_1 I_2$	0	$\frac{2}{\sqrt{3}} (\hat{\mathbf{i}} + i\hat{\mathbf{j}})$	$\frac{2}{\sqrt{3}} (\hat{\mathbf{i}} + i\hat{\mathbf{j}})$	0
$i \boldsymbol{\sigma}_1 \times \boldsymbol{\sigma}_2$	0	$-\frac{2}{\sqrt{3}} (\hat{\mathbf{i}} + i\hat{\mathbf{j}})$	$\frac{2}{\sqrt{3}} (\hat{\mathbf{i}} + i\hat{\mathbf{j}})$	0

In Refs. [11, 12], it was found that in the $\Lambda \rightarrow N\pi$ decays, there exists a “fine-tuning” cancellation mechanism for the two types of pole terms (type-A and type-B), even though the exclusive contributions from either type-A or type-B amplitude is sizeable. Interestingly, in the Ω decays, the ΛK^- channel involves only one type of pole term (strong interaction first, then weak interaction). The fact that this single pole term yields a substantial amplitude is consistent with the experimental observation that the ΛK^- mode has the largest branching ratio. We note in advance that the pole terms is indeed crucial for the decay $\Omega^- \rightarrow \Lambda K^-$ in order to reproduce the branching ratio of the experiment. On the one hand, it provides a clear evidence for the role played by the pole terms. On the other hand, it indicates that the pole terms are essential for understanding the underlying mechanisms of the Ω hyperon.

C. The nonrelativistic potential and baryon wave functions

In earlier theoretical work of Refs. [11, 19–22], a simple harmonic oscillator (H.O.) wave function was introduced to describe the motion of constituent quarks inside hadrons. During this process, a phenomenological parameter α was required, which inevitably made the cal-

culated results dependent on the choice of α . To address this issue, we adopt a numerical wave function based on the support of hadron spectroscopy. Specifically, we determine the parameters of the potential model by fitting existing hadron spectra, and then obtain the complete hadron wave function by solving the Schrödinger equation numerically. This approach yields a wave function that more faithfully represents the motion of constituent quarks and will reduce the uncertainty associated with the α parameter of the simple H.O. wave function.

To obtain the wave function of baryons in this work, we employ a non-relativistic Hamiltonian

$$H = \sum_{i=1}^3 \left(\frac{\mathbf{p}_i^2}{2m_i} + m_i \right) + \sum_{i < j} V(r_{ij}) + C_0, \quad (19)$$

to describe the baryon system, where $\mathbf{p}_i^2/(2m_i)$ is the kinetic energy of the i -th constituent quark with mass m_i and momentum \mathbf{p}_i , V_{ij} is the effective potential between the i -th and j -th quarks with a distance $r_{ij} \equiv |\mathbf{r}_i - \mathbf{r}_j|$. C_0 is the zero point energy. The effective potential can be decomposed into the spin-independent and spin-dependent parts,

$$V(r_{ij}) = V^{corn}(r_{ij}) + V^{sd}(r_{ij}). \quad (20)$$

The spin-independent part $V^{corn}(r_{ij})$ is adopted the well-

known Cornell form [23], i.e.,

$$V^{corn}(r_{ij}) = \frac{b_{ij}}{2}r_{ij} - \frac{2}{3}\frac{\alpha_{ij}}{r_{ij}}, \quad (21)$$

where the first term is the linear confinement potential V^{conf} , and the second term is the Coulomb-like potential V^{coul} derived from the one-gluon-exchange (OGE) model [24, 25]. b_{ij} and α_{ij} are the slope parameter of the confinement potential and strong coupling constant between the i -th and j -th quarks, respectively. While, the spin-dependent potentials in OGE model can be decomposed into

$$V^{sd}(r_{ij}) = V^{SS}(r_{ij}) + V^T(r_{ij}) + V^{LS}(r_{ij}), \quad (22)$$

where V^{SS} , V^T and V^{LS} stand for the spin-spin, tensor, and the spin-orbit potentials, respectively. The spin -spin and tensor potentials are given by

$$V^{SS}(r_{ij}) = \frac{2\alpha_{ij}}{3} \left\{ \frac{\pi}{2} \cdot \frac{\sigma_{ij}^3 e^{-\sigma_{ij}^2 r_{ij}^2}}{\pi^{3/2}} \cdot \frac{16}{3m_i m_j} (\mathbf{S}_i \cdot \mathbf{S}_j) \right\},$$

$$V^T(r_{ij}) = \frac{2\alpha_{ij}}{3m_i m_j r_{ij}^3} \left\{ \frac{3(\mathbf{S}_i \cdot \mathbf{r}_{ij})(\mathbf{S}_j \cdot \mathbf{r}_{ij})}{r_{ij}^2} - \mathbf{S}_i \cdot \mathbf{S}_j \right\}.$$

The spin-orbit potential contains a color-magnetic part and a Thomas-precession part [24, 26]

$$V^{LS}(r_{ij}) = V_{ij}^{so(\nu)} + V_{ij}^{so(s)}, \quad (23)$$

where these two parts $V_{ij}^{so(\nu)}$ and $V_{ij}^{so(s)}$ can be expressed as

$$V_{ij}^{so(\nu)} = \frac{1}{r_{ij}} \frac{dV_{ij}^{coul}}{dr_{ij}} \left(\frac{\mathbf{r}_{ij} \times \mathbf{p}_i \cdot \mathbf{S}_i}{2m_i^2} - \frac{\mathbf{r}_{ij} \times \mathbf{p}_j \cdot \mathbf{S}_j}{2m_j^2} \right. \\ \left. - \frac{\mathbf{r}_{ij} \times \mathbf{p}_j \cdot \mathbf{S}_i - \mathbf{r}_{ij} \times \mathbf{p}_i \cdot \mathbf{S}_j}{m_i m_j} \right),$$

$$V_{ij}^{so(s)} = -\frac{1}{r_{ij}} \frac{dV_{ij}^{conf}}{dr_{ij}} \left(\frac{\mathbf{r}_{ij} \times \mathbf{p}_i \cdot \mathbf{S}_i}{2m_i^2} - \frac{\mathbf{r}_{ij} \times \mathbf{p}_j \cdot \mathbf{S}_j}{2m_j^2} \right).$$

In the spin-dependent potentials, the S_i and \mathbf{p}_i are the spin and momentum operators of the i -th quark, respectively.

To obtain the masses and wave functions of baryons, we adopt the variation principle to solve the Schrödinger equation with the non-relativistic Hamiltonian

$$H|\Psi_{JJ_z}\rangle = E|\Psi_{JJ_z}\rangle, \quad (24)$$

in which the baryon wave function $|\Psi_{JJ_z}\rangle$ is constructed as a combination of color (ϕ_c), spin (χ_{SS_z}), spatial (ψ_{NLL_z}), and flavor (ϕ_f) terms:

$$\Psi_{JJ_z} = \mathcal{A}\{[\psi_{NLL_z}^\sigma(\boldsymbol{\rho}, \boldsymbol{\lambda}) \otimes \chi_{SS_z}^\sigma]_{JJ_z} \phi_f \phi_c\}, \quad (25)$$

where \mathcal{A} represents the operator that imposes the antisymmetry on the total wave function when the two light quarks are exchanged, and the spatial wave function $\psi_{NLL_z}^\sigma(\boldsymbol{\rho}, \boldsymbol{\lambda})$ consists of both ρ -mode and λ -mode excitations. We use the H.O. wave function bases, i.e.,

$$\psi_{n_\zeta l_\zeta m_\zeta}(\alpha_{\zeta\ell}, \zeta) = R_{n_\zeta l_\zeta}(\alpha_{\zeta\ell}, \zeta) Y_{l_\zeta m_\zeta}(\hat{\zeta}), \quad (26)$$

where $Y_{l_\zeta m_\zeta}(\hat{\zeta})$ ($\zeta = \rho, \lambda$) is the spherical harmonic function. The radial part $R_{n_\zeta l_\zeta}(\alpha_{\zeta\ell}, \zeta)$ in coordinate space can be written as

$$R_{n_\zeta l_\zeta}(\alpha_{\zeta\ell}, \zeta) = \alpha_{\zeta\ell}^{\frac{3}{2}} \left[\frac{2^{l_\zeta+2-n_\zeta} (2l_\zeta + 2n_\zeta + 1)!!}{\sqrt{\pi} n_\zeta! [(2l_\zeta + 1)!!]^2} \right]^{\frac{1}{2}} (\alpha_{\zeta\ell} \zeta)^l \\ \times e^{-\frac{1}{2} \alpha_{\zeta\ell}^2 \zeta^2} F(-n_\zeta, l_\zeta + \frac{3}{2}, \alpha_{\zeta\ell}^2 \zeta^2), \quad (27)$$

where $F(-n_\zeta, l_\zeta + \frac{3}{2}, \alpha_{\zeta\ell}^2 \zeta^2)$ is the confluent hypergeometric function. Using the Fourier transformation, the form of the radial part in momentum space is

$$R_{n_\zeta l_\zeta}(\alpha_{\zeta\ell}, p_\zeta) = (-1)^{n_\zeta} (-i)^{l_\zeta} \left[\frac{2^{l_\zeta+2-n_\zeta} (2l_\zeta + 2n_\zeta + 1)!!}{\sqrt{\pi} n_\zeta! [(2l_\zeta + 1)!!]^2} \right]^{\frac{1}{2}} \alpha_{\zeta\ell}^{-\frac{3}{2}} \left(\frac{p_\zeta}{\alpha_{\zeta\ell}} \right)^l e^{-\frac{p_\zeta^2}{2\alpha_{\zeta\ell}^2}} F(-n_\zeta, l_\zeta + \frac{3}{2}, \frac{p_\zeta^2}{\alpha_{\zeta\ell}^2}), \quad (28)$$

where $\alpha_{\zeta\ell}$ can be related to the H.O. frequency $\omega_{\zeta\ell}$ with $\alpha_{\zeta\ell} \equiv 1/d_{\zeta\ell} = \sqrt{M_\zeta \omega_{\zeta\ell}}$. The reduced masses $M_{\rho, \lambda}$ are defined by $M_\rho \equiv \frac{2m_1 m_2}{m_1 + m_2}$ and $M_\lambda \equiv \frac{3(m_1 + m_2)m_3}{2(m_1 + m_2 + m_3)}$. For a system with three identical quark [e.g., $\Omega(sss)$], one has $\alpha_{\lambda\ell} = \alpha_{\rho\ell}$. However, for systems consisting of two

identical quarks and another quark being different [e.g., $\Xi^0(ssu)$], the parameters of the two modes are not independent and their relationship is $\alpha_{\lambda\ell} = \alpha_{\rho\ell} \left(\frac{3m'}{2m+m'} \right)^{1/4}$. Taking into account that the constituent mass of a strange quark is close to that of a u/d quark the relation $d_{\lambda\ell} \simeq d_{\rho\ell}$ is a good approximation [15]. Thus, the

spatial wave function can be expanded as

$$\psi_{NLL_z}^\sigma(\rho, \lambda) = \sum_{\ell}^n C_\ell \psi_{NLL_z}^\sigma(d_\ell, \rho, \lambda). \quad (29)$$

Then, the Schrödinger equation can be solved by dealing with the generalized eigenvalue problem,

$$\sum_{\ell'=1}^n (H_{\ell\ell'} - EN_{\ell\ell'})C_{\ell'} = 0, \quad (30)$$

where $H_{\ell\ell'} \equiv \langle \xi(d'_\ell) | H | \xi(d_\ell) \rangle$ and $N_{\ell\ell'} \equiv \langle \xi(d'_\ell) | \xi(d_\ell) \rangle$, while the function $\xi(d_\ell)$ is given by

$$\xi(d_\ell) = \sum_{L_z+S_z=J_z} \langle LL_z; SS_z | JJ_z \rangle \psi_{NLL_z}^\sigma(d_\ell, \rho, \lambda) \chi_{SS_z}^\sigma.$$

In the calculations, the variational parameter d_ℓ is selected to form a geometric progression [27],

$$d_\ell = d_1 a^{\ell-1} (\ell = 1, \dots, n), \quad (31)$$

where n represents the number of basis functions, and a is the ratio coefficient. There are three parameters $\{d_1, d_n, n\}$ to be determined with the variation method. It is found that when taking $d_1 = 0.1$ fm, $d_n = 2$ fm, and $n = 10$, we can obtain stable results for the Ξ baryons.

TABLE IV: Quark model parameters used in this work.

b_{ss} (GeV 2)	α_{ss}	σ_{ss} (GeV)	m_s (GeV)	$m_{u/d}$ (GeV)
0.11	0.77	1.6	0.5	0.3
b_{us} (GeV 2)	α_{us}	σ_{us} (GeV)	C_0 (GeV)	
0.12	0.79	1.8	-0.619	

The parameters of the quark potential model adopted in this work have been presented in Tab. IV. The confinement strength b_{ss} and the strong coupling constant α_{ss} between two strange quarks are taken from Ref. [28], where they were determined by fitting the Ω mass spectrum. The constituent quark mass of the s quark and u/d quarks are fixed within their typical ranges. The others parameters of b_{us} , α_{us} , $\sigma_{ss/us}$ and C_0 are determined by an overall description of the masses of the four Ξ states in the PDG [3]: the 4-star states $\Xi(1415/1422)$ (where the numbers in parentheses represent the masses of the neutral and charged states respectively) and $\Xi(1535)$, together with the 3-star states $\Xi(1690)$ and $\Xi(1820)$. Although there is still controversy over the nature and even the J^P assignment of $\Xi(1690)$, as mentioned in Sec. II B, some experimental analyses confirm its quantum numbers of $J^P = \frac{1}{2}^-$. In addition, theoretical analysis based on the quark model suggests that it might be the first orbital excitation state $1^2P_{\frac{1}{2}-}$, although some calculations predict the $1^2P_{\frac{1}{2}-}$ mass to be slightly higher than the experimental $\Xi(1690)$ mass. The obtained mass spectra

for these four Ξ states compared with the data and some other works are given in Tab. V. We compare the obtained first orbital excitation state $1^2P_{\frac{1}{2}-}$ with $\Xi(1690)$ and its mass is higher than that of $\Xi(1690)$.

It is worth noting that the purpose of this work is not to determine the mass spectrum of Ξ baryons. Instead, we fit several experimentally well-established baryons to constrain the parameters of the quark potential model, which in turn allows us to obtain numerical wave functions for the Ξ states. The stability and rationality of these numerical wave functions are evaluated by comparing the obtained mass from solving the Schrödinger equation with the corresponding experimental values. The resulting numerical wave functions will be adopted in subsequent calculation of weak decays within the NRCQM, thereby reducing uncertainties introduced by additional phenomenological parameters.

III. THE HADRON-LEVEL AMPLITUDES AND FINAL STATE INTERACTIONS (FSIs)

One should be aware of the possible role played by the final state interactions (FSIs) in some hyperon hadronic weak decays. Regarding the puzzle of the branching ratios between $\Lambda \rightarrow p\pi^-$ and $\Lambda \rightarrow n\pi^0$, Ref. [11] considered the FSIs from $p\pi^-$ to $n\pi^0$ and found that this additional transition amplitude in $\Lambda \rightarrow n\pi^0$ can enhance the transition amplitude by interference and “coincidentally” retain the ratio of $BR(\Lambda \rightarrow p\pi^-)/BR(\Lambda \rightarrow n\pi^0) \simeq 2$ as observed in experiment.

In the above analysis of Eq. (7), it was pointed out that if only the $s \rightarrow u\bar{d}$ weak transition mechanism is considered, the predicted branching ratio of $\Omega^- \rightarrow \Xi^-\pi^0$ is approximately 1/18 of that for $\Omega^- \rightarrow \Xi^0\pi^-$, rather than the experimentally observed ratio of about 1/3 [4]. To account for this discrepancy, it is natural to consider possible enhancements to $\Omega^- \rightarrow \Xi^-\pi^0$ from FSIs. Notably, both $\Omega^- \rightarrow \Xi^0\pi^-$ and $\Omega^- \rightarrow \Lambda K^-$ exhibit relatively large branching fractions, which is consistent with the dominant DPE process in the former and a sizable pole term contribution in the latter—a fact already confirmed by experiment. As a result, the leading FSI correction to $\Omega^- \rightarrow \Xi^-\pi^0$ is expected to arise primarily from rescattering via the intermediate channels $\Xi^0\pi^-$ and ΛK^- . In turn, the rescattering contributions from $\Xi^-\pi^-$ to $\Xi^0\pi^-$ and ΛK^- should be much smaller and subleading since they originate from a tree-level amplitude that is already suppressed.

As illustrated in Fig. 2, we parameterize the contribution of FSIs via rescattering using this type of hadronic level triangle diagram. It should be noted in advance that the two-point bubble diagram related to the s -channel is not considered here, as the final calculation shows its correction to be negligible in this work. We employ the effective field theory approach to compute the loop-level amplitudes. The explicit Lagrangian forms for the above

TABLE V: The masses (MeV) of the Ξ baryons compared with the experimental data from the PDG [3] (labeled with Expt.) and the other theory predictions [16, 24, 29–35]. The values outside and inside the parentheses in the fourth column are the resonance masses without and with first order correction respectively in Ref [29]. The harmonic oscillator (H.O.) strength parameters α_ρ (GeV), given in the last column, are extracted by fitting a single H.O. form to our numerical wave functions, with the constraint that the root-mean-square radius of the ρ -mode excitations be reproduced.

$n^{2S+1}L_{JP}$	Ours	Ref. [24]	Ref. [29]	Ref. [30]	Ref. [31]	Ref. [32]	Ref. [33]	Ref. [16]	Ref. [34]	Ref. [35]	Expt. [3]	α_ρ
$1^2S_{\frac{1}{2}+}$	1319.2	1305	1322(1321)	1330	1310	1334	1318	1325	1317	1303 \pm 13	1315/1322	0.460
$1^4S_{\frac{3}{2}+}$	1530.0	1505	1531(1524)	1518	1539	1524	1539	1520	1526	1553 \pm 18	1535	0.373
$1^2P_{\frac{1}{2}-}$	1732.9	1755	1886(1889)	1682	1770	1869	1658	1725	1772	1716 \pm 43	1690?	0.463
$1^2P_{\frac{3}{2}-}$	1820.7	1785	1871(1873)	1764	1780	1828	1820	1759	1801	1906 \pm 29	1820	0.404

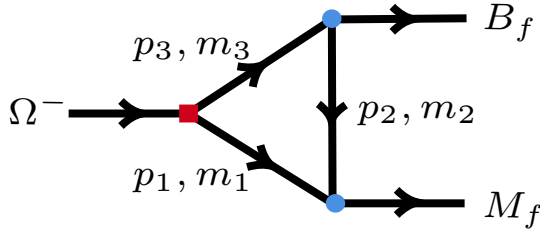


FIG. 2: Schematic diagram of the FSIs from the intermediate channel rescattering to $\Xi^- \pi^0$. Black squares and red dots represent weak and strong vertices respectively.

vertices can be written as

$$\mathcal{L}_{DBP} = ig_{DBP}^{(PC)} \bar{D}^\mu \partial_\mu P B \quad (32)$$

$$\mathcal{L}_{BBP} = i \frac{f_{BBP}}{m_P} \bar{B} \gamma_\mu \gamma_5 B \partial^\mu P, \quad (33)$$

$$\mathcal{L}_{BBV} = -g_{BBV} \bar{B} \gamma_\mu B V^\mu + \frac{f_{BBV}}{2m_B} \bar{B} \sigma^{\mu\nu} B \partial_\nu V_\mu, \quad (34)$$

$$\mathcal{L}_{VPP} = ig_{VPP} \langle (P \partial_\mu P - \partial_\mu P P) V_\mu \rangle, \quad (35)$$

where $\sigma^{\mu\nu} = i[\gamma^\mu, \gamma^\nu]/2$. D and B represent decuplet

baryon field with $J^P = \frac{3}{2}^+$ and octet baryon field with $J^P = \frac{1}{2}^+$, respectively; P and V represent pseudo-scalar meson with $J^P = 0^-$ and vector meson with $J^P = 1^-$, respectively.

The notation $[M1, M3, (M2)]$ is used to denote the intermediate interaction between particle $M1$ and $M3$ by exchanging $M2$. The masses and 4-vector momenta of these internal particles are denoted by (m_1, m_2, m_3) and (p_1, p_2, p_3) , respectively. The 4-vector momenta of the initial-state baryon, final-state baryon and final-state meson are labeled as p_i , p_f and p_M , respectively. In order to cut off the ultra-violet (UV) divergence in the loop integrals, we include a commonly-adopted form factor to regularize the loop integration:

$$\mathcal{F}(p_i^2) = \prod_i \left(\frac{\Lambda_i^2 - m_i^2}{\Lambda_i^2 - p_i^2} \right) \quad (36)$$

where $\Lambda_i = 1 \sim 2$ GeV as the cut-off parameter. As follow, we will write down the detailed amplitudes for each loop transition.

- $[\pi^-, \Xi^0, (\rho^+)]$ and $[K^-, \Lambda, (K^{*+})]$

$$i\mathcal{M} = g_1 g_2 g_3 \int \frac{d^4 p_1}{(2\pi)^4} \frac{p_{1\mu} (p_1 + p_M)_\nu (g^{\alpha\nu} - \frac{p_2^\alpha p_2^\nu}{p_2^2}) \bar{u}(p_f, \lambda_f) (\gamma_\alpha - \frac{f_3}{2m_B g_3} \frac{[\gamma_\alpha, \gamma_\beta]}{2} p_2^\beta) (p_3 + m_3) u^\mu(p_i, \lambda_i)}{(p_1^2 - m_1^2 + i\epsilon)(p_2^2 - m_2^2 + i\epsilon)(p_3^2 - m_3^2 + i\epsilon)} \mathcal{F}(p_i^2). \quad (37)$$

- $[\Xi^0, \pi^-, (\bar{\Xi}^0)]$ and $[\Lambda, K^-, (\bar{\Sigma}^0)]$

$$i\mathcal{M} = g_1 g_2 g_3 \int \frac{d^4 p_1}{(2\pi)^4} \frac{p_{3\mu} p_3^\nu p_M^\alpha \bar{u}(p_f, \lambda_f) \gamma_\alpha \gamma_5 \gamma_\nu \gamma_5 (\not{p}_1 + m_1) (\not{p}_2 + m_2) u^\mu(p_i, \lambda_i)}{(p_1^2 - m_1^2 + i\epsilon)(p_2^2 - m_2^2 + i\epsilon)(p_3^2 - m_3^2 + i\epsilon)} \mathcal{F}(p_i^2). \quad (38)$$

In these above decay amplitudes, we do not distinguish

the coupling constants at the hadronic vertices, but just

denote them as g_i ($i = 1, 2, 3$) for conciseness. $u^\mu(p, \lambda)$ represents the Rarita–Schwinger spinor of a spin-3/2 baryon with momentum p and helicity λ . It can be constructed from the Dirac spinor $u(p, \lambda)$ and the polarization vector $\epsilon^\mu(p, \lambda)$,

$$u^\mu(p, \lambda) = \sum_{\lambda_1, \lambda_2} \langle 1\lambda_1; \frac{1}{2}\lambda_2 | \frac{3}{2}\lambda \rangle \epsilon^\mu(p, \lambda_1) u(p, \lambda_2). \quad (39)$$

Next, we explain how the coupling constants of each vertex in the triangle loop shown in Fig. 2 are determined. Previous calculations indicate that the PV transition amplitude vanishes for $s \rightarrow u\bar{u}$ processes, and that the amplitude of $su \rightarrow u\bar{u}$ processes is significantly suppressed compared to the PC one. Therefore, both the amplitude of $s \rightarrow u\bar{u}$ and the amplitude of $su \rightarrow u\bar{u}$ are dominated by the PC transition, and we only consider the loop corrections of the PC transition here. The weak couplings $g_{\Omega\Xi^0\pi^-}^{(\text{PC})} = 1.37 \times 10^{-6} \text{ GeV}^{-1}$ and $g_{\Omega\Lambda K^-}^{(\text{PC})} = 3.98 \times 10^{-6} \text{ GeV}^{-1}$ are extracted from the tree processes illustrated in Fig. 1 and calculated within the NRCQM.

The coupling constants of the BBP and BBV vertices can be determined by the $\text{SU}(3)$ relationship,

$$\begin{aligned} f_{NN\pi} &= f_8^P, & f_{\Xi\pi} &= (1 - 2\alpha_{BBP})f_8^P, \\ f_{\Lambda\Xi K} &= \frac{1}{\sqrt{3}}(4\alpha_{BBP} - 1)f_8^P, \\ f_{\Lambda\Sigma\pi} &= \frac{2}{\sqrt{3}}(1 - \alpha_{BBP})f_8^P \quad (40) \\ g_{NN\rho} &= f_8^V, & g_{\Xi\rho} &= (1 - 2\alpha_{BBV}^e)g_8^V, \\ g_{\Lambda\Xi K^*} &= \frac{1}{\sqrt{3}}(4\alpha_{BBV}^e - 1)g_8^V, \end{aligned}$$

where the $f_8^P = f_{NN\pi} = 0.989$ [36] and $\alpha_{BBP} = 0.365$ [37] are used. For the vector coupling constant, we take $g_8^V = g_{NN\rho} = 3.25$ from the dispersion theory based on the meson exchange model [36]. The ratio α_{BBV}^e is determined by the relationship between the $NN\omega$ coupling $g_{NN\omega} = 15.83$ based on the Bonn model [38] and the coupling $g_{NN\rho}$: $\alpha_{BBV}^e = \frac{1}{4} \times (\frac{g_{NN\omega}}{g_{NN\rho}} + 1) = 1.47$, which is different from the value of 1 required by the universality of the quark model. As for the tensor coupling constant f_{BBV} , the Nijmegen model gives $f_{NN\rho} = 12.52$ [37] and the corresponding ratio α_{BBV}^m is usually fixed at 0.4 [39, 40], which is obtained by the $\text{SU}(6)$ symmetry. For the VPP vertices, the couplings $g_{\rho^+\pi^-\pi^0} = \sqrt{2}g_{VPP}$ and $g_{K^*+K^-\pi^0} = g_{VPP}/\sqrt{2}$ are extracted from the experimental data in $\rho \rightarrow \pi\pi$ and $K^* \rightarrow K\pi$ decays [41, 42]. These strong coupling constants of the BBP , BBV and VPP vertices used in this work are summarized in Tab. VI.

TABLE VI: The strong coupling constants of the BBP , BBV and VPP vertices.

BBP	$f_{\Xi\Xi\pi}$	$f_{\Sigma\Xi K}$	$f_{\Lambda\Sigma\pi}$
Values	0.267	0.989	0.725
BBV	$g_{\Xi\rho}$	$g_{\Lambda\Xi K^*}$	$f_{\Xi\Xi\pi}$ $f_{\Lambda\Xi K^*}$
Values	-6.31	9.16	10.86 -1.28
VPP	$g_{\rho^+\pi^-\pi^0}$	$g_{K^*+K^-\pi^0}$	
Values	5.96	3.30	

IV. THE DECAY WIDTH AND ASYMMETRY PARAMETER

In this work, the amplitudes of the DPE, CS, and pole terms are all calculated within the framework of the NRCQM, with mesons and baryons represented by mock states, respectively,

$$\begin{aligned} |\mathbb{M}(\mathbf{P}_c; J, J_z)\rangle &= \sum_{S_z, L_z; c_i} \langle LL_z; SS_z | JJ_z \rangle \int d\mathbf{p}_1 d\mathbf{p}_2 \\ &\times \delta^3(\mathbf{p}_1 + \mathbf{p}_2 - \mathbf{P}_c) \psi_{NLL_z}(\mathbf{p}_1, \mathbf{p}_2) \frac{\chi_{S_z, S_z}^{s_1, s_2} \delta_{c_1 c_2} \phi_{i_1 i_2}}{\sqrt{3}} \\ &\times b_{c_1, i_1, s_1, \mathbf{p}_1}^\dagger d_{c_2, i_2, s_2, \mathbf{p}_2}^\dagger |0\rangle, \quad (41) \end{aligned}$$

$$\begin{aligned} |\mathbb{B}(\mathbf{P}_c; J, J_z)\rangle &= \sum_{S_z, L_z; c_i} \langle LL_z; SS_z | JJ_z \rangle \int d\mathbf{p}_1 d\mathbf{p}_2 d\mathbf{p}_3 \\ &\times \delta^3(\mathbf{p}_1 + \mathbf{p}_2 + \mathbf{p}_3 - \mathbf{P}_c) \psi_{NLL_z}(\mathbf{p}_1, \mathbf{p}_2, \mathbf{p}_3) \chi_{S_z, S_z}^{s_1, s_2, s_3} \\ &\times \frac{\epsilon_{c_1 c_2 c_3}}{\sqrt{6}} \phi_{i_1 i_2 i_3} b_{c_1, i_1, s_1, \mathbf{p}_1}^\dagger b_{c_2, i_2, s_2, \mathbf{p}_2}^\dagger b_{c_3, i_3, s_3, \mathbf{p}_3}^\dagger |0\rangle, \quad (42) \end{aligned}$$

where c_j , s_j , i_j are color, spin, and flavor indexes, respectively. ψ_{NLL_z} is the spatial wavefunction which is taken as an harmonic oscillator wavefunction. \mathbf{p}_i denotes the single quark (antiquark) three-vector momentum, and \mathbf{P}_c (\mathbf{P}'_c) denotes the hadron momentum. χ_{S_z, S_z} is the spin wavefunction; ϕ is the flavor wavefunction, and $\delta_{c_1 c_2}/\sqrt{3}$ and $\epsilon_{c_1 c_2 c_3}/\sqrt{6}$ are the color wavefunctions for the meson and baryon, respectively. The normalization condition for the mock states are:

$$\begin{aligned} \langle \mathbb{M}(\mathbf{P}'_c; J, J_z) | \mathbb{M}(\mathbf{P}_c; J, J_z) \rangle &= \delta^3(\mathbf{P}'_c - \mathbf{P}_c), \\ \langle \mathbb{B}(\mathbf{P}'_c; J, J_z) | \mathbb{B}(\mathbf{P}_c; J, J_z) \rangle &= \delta^3(\mathbf{P}'_c - \mathbf{P}_c). \quad (43) \end{aligned}$$

In the above convention, for the two-body decay $A \rightarrow B + C$, the S -matrix is defined by

$$\mathcal{S} = \mathcal{I} - 2\pi i \delta^4(P_A - P_B - P_C) \tilde{\mathcal{M}}, \quad (44)$$

where

$$\delta^3(\mathbf{P}_A - \mathbf{P}_B - \mathbf{P}_C) \tilde{\mathcal{M}} \equiv \langle BC | H_I | A \rangle. \quad (45)$$

By integrating over phase space, the decay width can be expressed as:

$$\Gamma(A \rightarrow B + C) = \frac{8\pi^2 |\mathbf{k}| E_B E_C}{M_A} \frac{1}{2J_A + 1} \sum_{\text{spin}} |\tilde{\mathcal{M}}|^2, \quad (46)$$

where \mathbf{k} is the three-vector momentum of the final-state meson in the initial state rest frame, and J_A is the spin of the initial state. E_B and E_C are the energies of the final states B and C , respectively.

By redefining

$$\mathcal{M} \equiv 8\pi^{3/2}(M_A E_B E_C)^{1/2} \tilde{\mathcal{M}}, \quad (47)$$

where \mathcal{M} is the transition matrix element defined at the hadronic level, we can unify all the transition amplitudes as follows:

$$\mathcal{S} = 1 + i\mathcal{T} = 1 + (2\pi)^4 i\delta^4(P_A - P_B - P_C)\mathcal{M}. \quad (48)$$

In this convention, the expression for the decay width is:

$$\Gamma(A \rightarrow B + C) = \frac{|\mathbf{k}|}{8\pi M_A^2} \frac{1}{2J_A + 1} \sum_{J_i^z, J_f^z} \left(\left| \mathcal{M}_{(\text{PC})}^{J_i^z; J_f^z} \right|^2 + \left| \mathcal{M}_{(\text{PV})}^{J_i^z; J_f^z} \right|^2 \right), \quad (49)$$

where the helicity amplitudes have the following relationship:

$$\begin{aligned} \mathcal{M}_{(\text{PC})}^{\frac{3}{2}+\frac{1}{2}; \frac{1}{2}+\frac{1}{2}} &= -\mathcal{M}_{(\text{PC})}^{\frac{3}{2}-\frac{1}{2}; \frac{1}{2}-\frac{1}{2}} \\ \mathcal{M}_{(\text{PV})}^{\frac{3}{2}+\frac{1}{2}; \frac{1}{2}+\frac{1}{2}} &= +\mathcal{M}_{(\text{PV})}^{\frac{3}{2}-\frac{1}{2}; \frac{1}{2}-\frac{1}{2}}. \end{aligned} \quad (50)$$

We can also calculate the asymmetry parameters in our model. For the interest of understanding the transition mechanisms, we will focus on

$$\alpha = \frac{2\text{Re}(A^*B)}{|A|^2 + |B|^2} = \frac{2\text{Re}\left[(\mathcal{M}_{(\text{PV})}^{\frac{3}{2}-\frac{1}{2}; \frac{1}{2}-\frac{1}{2}})^* \mathcal{M}_{(\text{PC})}^{\frac{3}{2}-\frac{1}{2}; \frac{1}{2}-\frac{1}{2}}\right]}{|\mathcal{M}_{(\text{PV})}^{\frac{3}{2}-\frac{1}{2}; \frac{1}{2}-\frac{1}{2}}|^2 + |\mathcal{M}_{(\text{PC})}^{\frac{3}{2}-\frac{1}{2}; \frac{1}{2}-\frac{1}{2}}|^2},$$

where A and B represent the D -wave (PV) and P -wave (PC) amplitudes, respectively. It is obvious that α is bounded by $-1 \leq \alpha \leq 1$ and characterizes the relative strength between the PC and PV transitions.

V. RESULTS AND DISCUSSIONS

A. Parameters and inputs

Before presenting the numerical results, we clarify the parameters and inputs in our calculation as follows: the constituent quark masses for the u , d , and s quarks are taken as $m_u = m_d = 300$ MeV and $m_s = 500$ MeV, consistent with the values adopted in the potential model listed in Tab. IV; the masses of the Ξ baryon states are given by solving the Schrödinger equation in Sec. II C. Correspondingly, the numerical wave functions are also determined. For simplicity, the harmonic oscillator (H.O.) strength parameters α_ρ can be obtained by fitting a single H.O. form to our numerical wave functions, with the constraint that the root-mean-square radius of

TABLE VII: The tree-level amplitudes with $J_f^z = J_i^z = -1/2$ for different channels and the unit is 10^{-7} GeV.

$\mathcal{M}_T^{\frac{3}{2}-\frac{1}{2}; \frac{1}{2}-\frac{1}{2}}$	DPE(PC)	CS-1(PC)	CS-2(PC)	PT(PC)	PT(PV)
$\Omega^- \rightarrow \Xi^0 \pi^-$	-9.70	-	-	-	-
$\Omega^- \rightarrow \Xi^- \pi^0$	-	2.24	-	-	-
$\Omega^- \rightarrow \Lambda K^-$	-	-	1.43	-18.69	$-0.117 - 0.020i$

the ρ -mode excitations be reproduced. And the resulting values are listed in the last column of Tab. V.

For the initial Ω^- baryon, the H.O. parameters $\alpha_\rho = \alpha_\lambda = 0.455$ GeV can be obtained from Ref. [28], and this value was also derived by using the numerical wave function given in this literature to fit the single H.O. wave function. For the decay channel $\Omega^- \rightarrow \Lambda K^-$, the ρ -mode H.O. parameter of the final baryon Λ is taken as $\alpha_\rho = 0.447$ GeV from Ref. [11], while the λ -mode H.O. parameter α_λ in a system with non-identical quarks is related to the ρ -mode parameter with the following relation

$$\alpha_\lambda = \left(\frac{3m'}{m + m + m'} \right)^{1/4} \alpha_\rho, \quad (51)$$

where m' represents the mass of the quark that differs from the other two, for example, in the case of the Λ baryon, $m' = m_s$.

The pion wave function is also expressed as a H.O. form with a parameter R . Since the pion is extremely light and associated with the spontaneous chiral symmetry breaking, it favors a larger value for R , and turns out to have a broad distribution in the momentum space [43]. A larger value for R also manifests that the relativistic effects become predominant in such a light quark system. In this work, $R = 0.53$ GeV was adopted, and this treatment is empirical and inevitably carries some intrinsic uncertainty. However, we would like to investigate the uncertainty by varying the parameter R within a reasonable range in the subsequent numerical results and discuss the phenomenological consequences.

The intermediate states of the pole terms are Ξ resonances in the decay $\Omega^- \rightarrow \Lambda K^-$, as illustrated in Fig. 1 (d). The states with $J^P = \frac{1}{2}^+$ and $J^P = \frac{1}{2}^-$ contribute to the PC and PV transition processes, respectively. To be more specific, we consider the ground state $1^2S_{\frac{1}{2}^+}$ and the first orbital excitation state $1^2P_{\frac{1}{2}^-}$ whose masses and wave functions are determined from the quark potential model and listed in Tab. V.

B. Numerical results and discussions

We first calculate the tree-level amplitudes for the DPE, CS and PT processes, which are summarized in Tab. VII. It should be noted that for all $s \rightarrow u\bar{u}$ weak processes, the PV transition amplitudes vanish; hence, they are not included the table. As clearly shown in

TABLE VIII: The loop amplitudes with $J_f^z = J_i^z = -1/2$ for $\Omega^- \rightarrow \Xi^0 \pi^-$ at two different values of Λ and the unit is 10^{-8} GeV.

$\mathcal{M}_L^{\frac{3}{2}-\frac{1}{2};\frac{1}{2}-\frac{1}{2}}$	$[\pi^-, \Xi^0, (\rho^+)]$	$[K^-, \Lambda, (K^{*+})]$	$[\Xi^0, \pi^-, (\Xi^0)]$	$[\Lambda, K^-, (\Xi^0)]$
$\Lambda = 1.5 \text{ GeV}$	$9.25 - 6.14i$	$-5.32 - 11.89i$	$0.008 - 0.03i$	$0.026 - 0.38i$
$\Lambda = 2.0 \text{ GeV}$	$10.68 - 18.92i$	$-6.74 - 16.84i$	$0.006 - 0.14i$	$0.020 - 1.00i$

Tab. II, the vanishing PV amplitude stems from the fact that all corresponding spin matrix elements are zero. A notable feature is that the DPE process contributes exclusively to $\Omega^- \rightarrow \Xi^0 \pi^-$. This exclusivity arises because the $s\bar{u}$ quark pair produced at the weak vertex can hadronize directly into the final-state π^- meson (see Fig. 1(d)). This direct hadronization mechanism implies no color suppression for the DPE amplitude, which consequently explains its larger magnitude compared to the CS amplitude.

We then focus on the two decay channels, $\Omega^- \rightarrow \Xi^0 \pi^-$ and $\Omega^- \rightarrow \Xi^- \pi^0$. Eq. (7) implies that, if only the $s \rightarrow u\bar{d}$ mechanism is considered, the ratio of their branching ratios would be approximately

$$BR_{\text{DPE}}(\Omega^- \rightarrow \Xi^0 \pi^-) \simeq 18 BR_{\text{CS}}(\Omega^- \rightarrow \Xi^- \pi^0). \quad (52)$$

This prediction, however, is in serious disagreement with the experimental data. As shown in Tab. IX, the calculated branching ratio for $\Xi^0 \pi^-$ agrees with experiment, which necessarily means that the result for $\Xi^- \pi^0$ lies significantly below the measured value. In our calculation, the branching ratio of the $\Xi^- \pi^0$ channel contributed by the CS process as shown in Fig. 1 is 1.29%, which is consistent with the relationship in Eq. (52).

The large difference in the branching ratios between $\Omega^- \rightarrow \Xi^- \pi^0$ and $\Xi^0 \pi^-$ is mainly because of the absence of the DPE process in the former channel. However, the decay $\Omega^- \rightarrow \Lambda K^-$ also lacks a DPE contribution, yet its experimentally measured branching ratio is sizable, at approximately 66%. Our analysis reveals that this channel receives a dominant contribution from pole terms. Specifically, only one type of pole diagram is relevant here, characterized by a strong interaction occurs first and then a weak interaction follows (see Fig. 1(d)). In our calculation, the intermediate poles we considered are the Ξ baryons of the $1^2S_{\frac{1}{2}+}$ and $1^2P_{\frac{1}{2}-}$ states, corresponding to the PC and PV transition, respectively. As shown in Tab. VII, the amplitude from the pole terms is much larger than that of the CS in this channel, thereby enhancing its predicted branching ratio. To be more specific, the decay $\Omega^- \rightarrow \Lambda K^-$ is dominated by the pole process of the PC transition, as the PV amplitude is much smaller than the PC amplitude. This also indicates that it is reasonable to ignore the contribution from higher excitation states.

After including both the $s \rightarrow u\bar{d}$ mechanism through W -emission (DPE and CS) and the $su \rightarrow ud$ mechanism via W -exchange (PT) at the quark level, we calculate the branching ratios and asymmetry parameters for

the decays $\Omega^- \rightarrow \Xi \pi$ and ΛK^- . Our results show that the branching ratios for $\Omega^- \rightarrow \Xi^0 \pi^-$ and ΛK^- channels are in good agreement with the experimental data presented in Tab. IX, while a significant discrepancy persists for $\Omega^- \rightarrow \Xi^- \pi^0$ whose predicted branching ratio is only 1.29%—are below the measured value.

Moreover, the asymmetry parameters for both $\Omega^- \rightarrow \Xi^0 \pi^-$ and $\Xi^- \pi^0$ are predicted to be zero, due to the vanishing PV amplitudes in their DPE or CS processes. In $\Omega^- \rightarrow \Lambda K^-$, however, the pole terms mechanism introduce a small non-zero PV amplitude, resulting in a very small but non-zero asymmetry parameter. All three decays are found to be dominated by parity-conserving (P -wave) transitions, which is consistent with experimental measurements that report asymmetry parameters very close to zero. Ref. [44] also expects the D -wave component (related to PV transition) to be very small. Notably, for the $\Omega^- \rightarrow \Xi^0 \pi^-$ and $\Xi^- \pi^0$ channels, the experimental uncertainties of asymmetry parameters are larger than the central values themselves, meaning our predictions lie well within the allowed experimental ranges.

For the decay $\Omega^- \rightarrow \Xi^- \pi^0$, the branching ratio predicted from the CS process alone remains in disagreement with experiment. This discrepancy arises because the CS amplitude is significantly smaller than those of the DPE or pole terms, which dominate $\Omega^- \rightarrow \Xi^0 \pi^-$ and ΛK^- , respectively. Given the much larger amplitude for $\Omega^- \rightarrow \Xi^0 \pi^-/\Lambda K^-$ than $\Omega^- \rightarrow \Xi^- \pi^0$, and the closeness of these thresholds, FSIs via rescattering processes such as $\Omega^- \rightarrow \Xi^0 \pi^-/\Lambda K^- \rightarrow \Xi^- \pi^0$ may provide a sizable correction.

We therefore consider the FSI contributions through the triangle process shown in Fig. 2, while neglecting the two-point bubble loop mentioned in Ref. [11], as our results shows that their contributions to be negligible. Since the PV amplitudes in the DPE and pole process are very small or even zero, we consider only FSIs in the PC transition process. Treating FSIs as an additional mechanism that can significantly enhance $\Omega^- \rightarrow \Xi^- \pi^0$, we present the calculated helicity amplitudes of each hadronic loop in Tab. VIII with the cut-off parameter $\Lambda = 1.5 \text{ GeV}$ and 2 GeV adopted. The results in Tab. VIII show that the first two loop amplitudes are at the same order of magnitude as the tree-level CS amplitude listed in Tab. VII for $\Omega^- \rightarrow \Xi^- \pi^0$.

By incorporating these FSIs, we plot the branching ratio of $\Omega^- \rightarrow \Xi^- \pi^0$ as a function of Λ , finding that for $\Lambda \simeq 1.9 \text{ GeV}$, the predicted branching ratio agrees with the experimental value, as shown in Tab. IX. This consistency supports the interpretation that FSIs constitute the essential missing ingredient in a unified theoretical description of the $\Omega^- \rightarrow \Xi^- \pi^0$ partial width.

As a result, our calculations of the branching ratios and the asymmetry parameters are presented in Tab. IX. These results are compared with the experimental data and the predictions from other theoretical models. It can be observed that our results for the branching ratios are in good agreement with the latest results from BESIII [4].

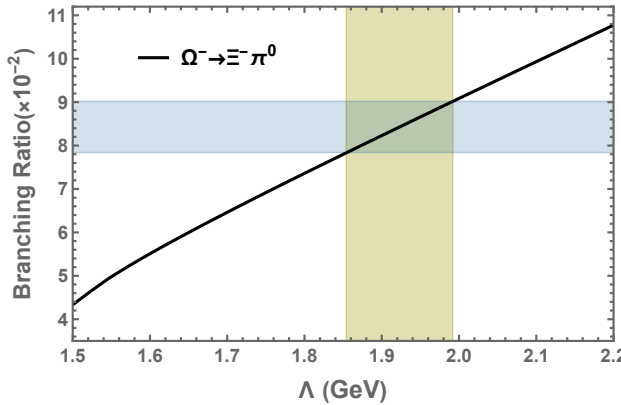


FIG. 3: The obtained branching ratio of $\Omega^- \rightarrow \Xi^- \pi^0$ as a function of the cut-off parameter Λ , comparing with the experimental data (horizontal blue bands). The vertical dark yellow band indicates the range where our results overlap with the experimental data.

We look forward to BESIII making more precise measurements of the asymmetric parameters. We also examine the uncertainty of the results introduced by the H.O. parameter R of the pion meson. The $\Xi^0 \pi^-$ and ΛK^- channels are respectively dominated by the DPE process and the PT process. By including the FSI contributions through the rescattering processes $\Xi^0 \pi^- / \Lambda K^- \rightarrow \Xi^- \pi^0$, the branching ratio of the $\Xi^- \pi^0$ channel is significantly enhanced. Consequently, the results of $\Xi^- \pi^0$ and ΛK^- channels show little dependence on the H.O. parameter R of the pion, whereas the $\Xi^0 \pi^-$ result is more sensitive to it. We observe that when $R = 0.53 \pm 0.053$, the resulting branching ratio uncertainty for $\Xi^0 \pi^-$ is $(24.52 \pm 7.35)\%$. This level of uncertainty is reasonable and acceptable within the typical parameter dependence of the quark-model calculations.

VI. SUMMARY

In this work, we have performed a systematic study of the singly Cabibbo-suppressed hadronic weak decays of the Ω^- hyperon, specifically the $\Omega^- \rightarrow \Xi^0 \pi^-$, $\Xi^- \pi^0$, and ΛK^- channels. Within the framework of the NRCQM, we first calculated the tree-level amplitudes for the DPE, CS, and PT processes arising from the quark-level transitions $s \rightarrow u\bar{u}$ and $su \rightarrow ud$. In our calculations, we employ the numerical wave function of baryons based on spectroscopic support to extract the H.O. parameters, which will reduce the uncertainty of observables associated with phenomenological parameter inputs.

The DPE process, due to the absence of color suppression, clearly plays a dominant role. This results in the branching ratio of the $\Xi^0 \pi^-$ channel being much larger than that of the $\Xi^- \pi^0$. Therefore, when the branching ratio of $\Xi^0 \pi^-$ is consistent with the experiment, $\Xi^- \pi^0$ inevitably deviates significantly from the experimental data. On the other hand, the large branching fraction of

$\Omega^- \rightarrow \Lambda K^-$ is successfully reproduced by the dominant contribution from the pole terms involving intermediate Ξ resonances ($1^2S_{\frac{1}{2}}$ and $1^2P_{\frac{1}{2}}$ states).

Considering both the $s \rightarrow u\bar{u}$ (W -emission) and $su \rightarrow ud$ (W -exchange) weak mechanisms, our results show that they cannot simultaneously describe the experimental branching ratios of these three channels. The main discrepancy lies in the $\Xi^- \pi^-$ channel, whose predicted branching ratio is significantly underestimated due to the much smaller amplitude of the CS process compared to the dominant DPE and pole term amplitudes.

To resolve these discrepancies, we introduced a key non-perturbative dynamical mechanisms—final state interactions (FSIs). We find the deficit in the predicted branching ratio for $\Omega^- \rightarrow \Xi^- \pi^0$ can be remedied by incorporating the FSIs which occurs in the form of rescattering process. Specifically, we computed the loop amplitudes via triangle diagrams from the $\Xi^0 \pi^-$ and ΛK^- intermediate states into the $\Xi^- \pi^0$ final state. With the inclusion of the FSI contributions, our theoretical predictions for the branching ratios and asymmetry parameters of all three decay channels achieve excellent agreement with the latest experimental data from BESIII [4]. This demonstrates that a consistent theoretical description of Ω^- decays requires a comprehensive picture that integrates quark-level weak vertices, baryon pole structures, and hadron-level final-state rescattering effects. Our analysis highlights the significant role played by FSIs as the essential missing piece for understanding the $\Omega^- \rightarrow \Xi^- \pi^0$ decay width, providing a unified framework for the hadronic weak decays of the Ω^- hyperon.

In brief, we find that a consistent description of all three decay channels emerges only when the following elements are combined: (i) The large ΛK^- rate is dominated by one type of pole term since there is no cancellation. (ii) The $\Xi^0 \pi^-$ rate is well-described by the direct, color-allowed weak transition. (iii) The observed $\Xi^- \pi^0$ rate is reproduced through significant constructive interference between the color suppressed tree amplitude and the FSI amplitudes fed from the $\Xi^0 \pi^-$ and ΛK^- channels. Our results provide a unified picture of Ω^- hadronic weak decays, demonstrating the indispensable role of non-perturbative long-distance dynamics. The weak decays of Ω^- provide important information about the interplay between the strong and weak interactions that is complementary to the weak decays of the ground-state spin-1/2 octet baryons.

Acknowledgments

We would like to thank Dr. Hui-Hua Zhong for useful discussions on solving the numerical wave function of baryons. This work is partly supported by the National Key R&D Program of China under Grant No. 2023YFA1606703, and by the National Natural Science Foundation of China under Grant Nos. 12575094, 12435007, 12361141819 and 12235018. This work is also

TABLE IX: Our results of branching ratio (BR) and asymmetry parameter (AP) for the decays $\Omega^- \rightarrow \Xi\pi$ and ΛK^- compared with the experimental data [3, 4] (labeled with Expt.) and the other theory predictions [6, 8, 10]. For $\Omega^- \rightarrow \Xi^-\pi^0$, the values listed in the fourth column are the results with the contribution of FSIs corresponding to the cut-off parameter $\Lambda = 1.9$ GeV.

		$\Omega^- \rightarrow \Xi^0\pi^-$	$\Omega^- \rightarrow \Xi^-\pi^0$	$\Omega^- \rightarrow \Lambda K^-$
BR(%)	Ours	24.52	8.23	65.83
	Expt. [4]	$25.03 \pm 0.44 \pm 0.53$	$8.43 \pm 0.52 \pm 0.28$	$66.3 \pm 0.8 \pm 2.0$
	Ref. [10]	34.67	5.36	67.98
	Ref. [6]	17.18	8.59	78.94
	Ref. [8]	20.21	9.48	69.98
AP	Ours	0	0	0.0121
	Expt. [3]	0.09 ± 0.14	0.05 ± 0.21	0.0154 ± 0.002
	Ref. [8]	0	0	-0.015

supported by the Gansu Province Postdoctor Foundation.

Appendix A: The wave function of hadrons

The flavor and spin wave function can be constructed respectively through the $SU(3)$ and $SU(2)$ symmetries. For the three quark systems, the direct product decomposition of the flavor $SU(3)$ symmetry is $\mathbf{3} \otimes \mathbf{3} \otimes \mathbf{3} = \mathbf{10}^s \oplus \mathbf{8}^{\rho} \oplus \mathbf{8}^{\lambda} \oplus \mathbf{1}^a$. Therefore, for the ground-state baryons, there will be a completely symmetric decuplet with $J^P = \frac{3}{2}^+$ and a mixed-symmetry octet with $J^P = \frac{1}{2}^+$. Combining together the spin and flavor symmetry, the spin-flavor wave functions follow an $SU(6)$ symmetry and usually denoted by $|N_6, 2S+1 N_3\rangle$ in the literature, where N_6 and N_3 represent the dimensions of the $SU(6)$ and $SU(3)$ representations, respectively, and S stands for the quantum number of the total spin of a baryon state.

The spatial wave functions satisfy the $O(3)$ symmetry under a rotation transformation. For a baryon system containing three quarks, the spatial wave function $\psi_{NLLz}^{\sigma} = [\psi_{n_{\rho}l_{\rho}m_{\rho}}(\mathbf{p}_{\rho}) \otimes \psi_{n_{\lambda}l_{\lambda}m_{\lambda}}(\mathbf{p}_{\lambda})]_{NLLz}$ is composed of ρ - and λ - mode spatial wave functions. The quantum numbers n_{ρ} , l_{ρ} and m_{ρ} [or n_{λ} , l_{λ} , m_{λ}] stand for that for the radial excitation, relative orbital angular momentum and its z component for the ρ -mode [or λ -mode] wavefunction, respectively. While N , L and L_z stand for the principal quantum number, the quantum numbers of total orbital angular momentum and its z component, respectively. They are defined by $N = 2(n_{\rho} + n_{\lambda}) + l_{\rho} + l_{\lambda}$, $|l_{\rho} - l_{\lambda}| \leq L \leq l_{\rho} + l_{\lambda}$ and $L_z = m_{\rho} + m_{\lambda}$. Furthermore, the superscript σ appearing in wave functions represents their permutation symmetries.

The total wave functions of a baryon can be expressed as $|qqq\rangle_A = |\text{color}\rangle_A \otimes |\text{spin, flavor, spatial}\rangle_S$. Based on the requirement of the $SU(6) \otimes O(3)$ symmetry, one can obtain the configurations for the spin-flavor-spatial part. Specially, the total wavefunction with quantum number $J^P = \frac{3}{2}^+$ and $J^P = \frac{1}{2}^{\pm}$ denoted by

$|N_6, 2S+1 N_3, N, \mathbf{L}, \mathbf{J}^P\rangle$ can be constructed as follows:

$$|56, 4 10, 0, 0, \frac{3}{2}^+ \rangle = \phi^s \chi^s \psi_{000}^s, \quad (A1)$$

$$|56, 2 8, 0, 0, \frac{1}{2}^+ \rangle = \frac{1}{\sqrt{2}} (\phi^{\rho} \chi^{\rho} + \phi^{\lambda} \chi^{\lambda}) \psi_{000}^s, \quad (A2)$$

$$|70, 2 8, 1, 1, \frac{1}{2}^- \rangle = \sum_{L_z + S_z = J_z} \langle 1L_z; \frac{1}{2}S_z | \frac{1}{2}J_z \rangle \times \frac{1}{2} [(\phi^{\rho} \chi^{\lambda} + \phi^{\lambda} \chi^{\rho}) \psi_{11L_z}^{\rho} + (\phi^{\rho} \chi^{\rho} - \phi^{\lambda} \chi^{\lambda}) \psi_{11L_z}^{\lambda}] \quad (A3)$$

$$|70, 2 8, 1, 1, \frac{3}{2}^- \rangle = \sum_{L_z + S_z = J_z} \langle 1L_z; \frac{1}{2}S_z | \frac{3}{2}J_z \rangle \times \frac{1}{2} [(\phi^{\rho} \chi^{\lambda} + \phi^{\lambda} \chi^{\rho}) \psi_{11L_z}^{\rho} + (\phi^{\rho} \chi^{\rho} - \phi^{\lambda} \chi^{\lambda}) \psi_{11L_z}^{\lambda}] \quad (A4)$$

$$|70, 4 8, 1, 1, \frac{1}{2}^- \rangle = \sum_{L_z + S_z = J_z} \langle 1L_z; \frac{3}{2}S_z | \frac{1}{2}J_z \rangle \times \frac{1}{\sqrt{2}} [\phi^{\rho} \chi^s \psi_{11L_z}^{\rho} + \phi^{\lambda} \chi^s \psi_{11L_z}^{\lambda}]. \quad (A5)$$

The wave function of pseudoscalar mesons is written as

$$\Phi_{000}(\mathbf{p}_1, \mathbf{p}_2) = \delta^3(\mathbf{p}_1 + \mathbf{p}_2 - \mathbf{P}) \phi_P \chi_{0,0}^a \psi_{000}^s(\mathbf{p}_1, \mathbf{p}_2), \quad (A6)$$

where $\chi_{0,0}^s$ is the wave function:

$$\chi_{0,0}^a = \frac{1}{\sqrt{2}} (\uparrow\downarrow - \downarrow\uparrow), \quad (A7)$$

and ϕ_P is the flavor wave function and we adopt the de Swart's convention [45]:

$$(\phi_{\pi^+}, \phi_{\pi^0}, \phi_{\pi^-}) = \left(-u\bar{d}, \frac{u\bar{u} - d\bar{d}}{\sqrt{2}}, d\bar{u} \right), \quad (A8)$$

$$(\phi_{K^+}, \phi_{K^0}, \phi_{\bar{K}^0}, \phi_{K^-}) = \left(u\bar{s}, d\bar{s}, s\bar{d}, -s\bar{u} \right), \quad (A9)$$

$$\phi_{\eta_8} = \frac{1}{\sqrt{6}} (u\bar{u} + d\bar{d} - 2s\bar{s}), \quad (A10)$$

$$\phi_{\eta_1} = \frac{1}{\sqrt{3}} (u\bar{u} + d\bar{d} + s\bar{s}). \quad (A11)$$

The spatial wave function is expressed as:

$$\psi_{000}^s(\mathbf{p}_1, \mathbf{p}_2) = \frac{1}{\pi^{3/4} R^{3/2}} \exp \left[-\frac{(\mathbf{p}_1 - \mathbf{p}_2)^2}{8R^2} \right], \quad (\text{A12})$$

where R is the harmonic oscillator strength parameter of mesons.

Appendix B: Transition amplitudes extracted in the quark model

For convenience, the analytical transition amplitudes obtained using the H.O. wave functions is presented be-

low. The amplitudes are expressed in terms of the baryon polarization quantum numbers. In the following expressions, $\mathcal{M}^{J_i J_i^z; J_f J_f^z}$ is abbreviated as $\mathcal{M}^{J_i^z; J_f^z}$; m_q denotes the mass of the u/d quarks and m_s the mass of the s quark; \mathbf{k} and ω_0 represent the three-vector momentum and energy of the final meson, respectively. To distinguish the H.O. parameters of different hyperons, we label them according to the number of strange quarks in the baryon: Specifically, the H.O. parameter of Ω is α_{sss} , that of Ξ is $\alpha_{ss\rho}$ and $\alpha_{ss\lambda}$, and that of Λ is $\alpha_{s\rho}$ and $\alpha_{s\lambda}$.

$$\bullet \Omega^- \rightarrow \Xi^0 \pi^-$$

$$\mathcal{M}_{\text{DPE,PC}}^{-\frac{1}{2}; -\frac{1}{2}} = -\frac{8G_F V_{ud} V_{us} |\mathbf{k}|}{\sqrt{3} \pi^{9/4}} \left(\frac{R \alpha_{sss}^2 \alpha_{ss\lambda} \alpha_{ss\rho}}{\alpha_{sss}^2 + \alpha_{ss\rho}^2} \right)^{3/2} \frac{m_q \alpha_{ss\lambda}^2 + m_s (\alpha_{sss}^2 + 2\alpha_{ss\lambda}^2)}{m_q (m_q + 2m_s) (\alpha_{sss}^2 + \alpha_{ss\lambda}^2)^{5/2}} \times \exp \left[-\frac{3m_s^2 \mathbf{k}^2}{(m_q + 2m_s)^2 (\alpha_{sss}^2 + \alpha_{ss\lambda}^2)} \right], \quad (\text{B1})$$

$$\mathcal{M}_{\text{DPE,PV}}^{-\frac{1}{2}; -\frac{1}{2}} = 0. \quad (\text{B2})$$

$$\bullet \Omega^- \rightarrow \Xi^- \pi^0$$

$$\mathcal{M}_{\text{CS-1,PC}}^{-\frac{1}{2}; -\frac{1}{2}} = \frac{4\sqrt{6}G_F V_{ud} V_{us} |\mathbf{k}|}{9\pi^{9/4}} \left(\frac{\alpha_{sss}^2 \alpha_{ss\rho} \alpha_{ss\lambda} R}{\alpha_{sss}^2 + \alpha_{ss\rho}^2} \right)^{3/2} \frac{m_q \alpha_{ss\lambda}^2 + m_s (\alpha_{sss}^2 + 2\alpha_{ss\lambda}^2)}{m_q (m_q + 2m_s) (\alpha_{sss}^2 + \alpha_{ss\lambda}^2)^{5/2}} \times \exp \left[-\frac{3m_s^2 \mathbf{k}^2}{(m_q + 2m_s) (\alpha_{sss}^2 + \alpha_{ss\lambda}^2)} \right], \quad (\text{B3})$$

$$\mathcal{M}_{\text{CS-1,PV}}^{-\frac{1}{2}; -\frac{1}{2}} = 0. \quad (\text{B4})$$

$$\bullet \Omega^- \rightarrow \Lambda K^-$$

$$\mathcal{M}_{\text{CS-2,PC}}^{-\frac{1}{2}; -\frac{1}{2}} = \frac{12\sqrt{6}G_F V_{ud} V_{us} |\mathbf{k}| (R \alpha_{sss}^2 \alpha_{s\lambda} \alpha_{s\rho})^{3/2} ((m_q + m_s) R^2 + m_q \alpha_{sss}^2) ((3m_q + m_s) \alpha_{sss}^2 + 2(2m_q + m_s) \alpha_{s\lambda}^2)}{\pi^{9/4} m_q (m_q + m_s) 2m_q + m_s (3\alpha_{sss}^4 + 4\alpha_{sss}^2 \alpha_{s\lambda}^2 + 6R^2 (\alpha_{sss}^2 + \alpha_{s\lambda}^2))^{5/2}} \times \exp \left[-\frac{3m_s^2 \mathbf{k}^2 (6m_q m_s (R^2 + \alpha_{sss}^2) + 8m_q m_s \alpha_{s\lambda}^2 + m_q^2 (3R^2 + 6\alpha_{sss}^2 + 8\alpha_{s\lambda}^2) + m_s^2 (3R^2 + 2(\alpha_{sss}^2 + \alpha_{s\lambda}^2)))}{2(m_q + m_s)^2 (2m_q + m_s)^2 (3\alpha_{sss}^4 + 4\alpha_{sss}^2 \alpha_{s\lambda}^2 + 6R^2 (\alpha_{sss}^2 + \alpha_{s\lambda}^2)^2)} \right], \quad (\text{B5})$$

$$\mathcal{M}_{\text{CS-2,PV}}^{-\frac{1}{2}; -\frac{1}{2}} = 0, \quad (\text{B6})$$

$$\begin{aligned}
\mathcal{M}_{\text{PT,PC}}^{-\frac{1}{2};-\frac{1}{2}}[\Xi^0(\frac{1}{2}^+)] &= \frac{2\sqrt{6}|\mathbf{k}|(2m_q(m_q+2m_s)(\alpha_{sss}^2+\alpha_{ss\lambda}^2)-m_q\alpha_{sss}^2\omega_0+(m_q+2m_s)\alpha_{ss\lambda}^2\omega_0)(\alpha_{sss}^2\alpha_{ss\lambda}\alpha_{ss\rho})^{3/2}}{3\pi^{3/2}f_K\sqrt{\omega_0}m_q(m_q+2m_s)(\alpha_{sss}^2+\alpha_{ss\lambda}^2)^{5/2}(\alpha_{sss}^2+\alpha_{ss\rho}^2)^{3/2}} \\
&\times \exp\left[-\frac{3m_s^2\mathbf{k}^2}{(m_q+2m_s)^2(\alpha_{sss}^2+\alpha_{ss\lambda}^2)}\right] \frac{2m_\Xi}{m_\Lambda^2-m_\Xi^2+im_\Xi\Gamma_\Xi} \frac{16\sqrt{3}GV_{ud}V_{us}}{\pi^{3/2}} \left(\frac{\alpha_{s\lambda}\alpha_{s\rho}\alpha_{ss\lambda}\alpha_{ss\rho}}{\alpha_{ss\lambda}^2+3\alpha_{ss\rho}^2+4\alpha_{s\lambda}^2}\right)^{3/2} \\
&\times \exp\left[-\frac{3m_s^2(m_q-m_s)^2\mathbf{k}^2}{(2m_q+m_s)^2(m_q+2m_s)^2(\alpha_{ss\lambda}^2+3\alpha_{ss\rho}^2+4\alpha_{s\lambda}^2)}\right], \tag{B7}
\end{aligned}$$

$$\begin{aligned}
\mathcal{M}_{\text{PT,PV}}^{-\frac{1}{2};-\frac{1}{2}}[\Xi^0(\frac{1}{2}^-)] &= \frac{-i4\mathbf{k}^2m_s\alpha_{sss}^3\alpha_{ss\rho}^{3/2}\alpha_{ss\lambda}^{5/2}(2m_q(m_q+2m_s)(\alpha_{sss}^2+\alpha_{ss\lambda}^2)-m_q\alpha_{sss}^2\omega_0+(m_q+2m_s)\alpha_{ss\lambda}^2\omega_0)}{\sqrt{3}\pi^{3/2}f_K\sqrt{\omega_0}m_q(m_q+2m_s)(\alpha_{sss}^2+\alpha_{ss\rho}^2)^{3/2}(\alpha_{sss}^2+\alpha_{ss\lambda}^2)^{7/2}} \\
&\times \exp\left[-\frac{3m_s^2\mathbf{k}^2}{(m_q+2m_s)^2(\alpha_{sss}^2+\alpha_{ss\lambda}^2)}\right] \frac{2m_\Xi}{m_\Lambda^2-m_\Xi^2+im_\Xi\Gamma_\Xi} \frac{i8\sqrt{2}GV_{ud}V_{us}}{\pi^{3/2}} \frac{(\alpha_{s\rho}\alpha_{s\lambda}\alpha_{ss\rho}\alpha_{ss\lambda})^{3/2}}{(\alpha_{ss\lambda}^2+3\alpha_{ss\rho}^2+4\alpha_{s\lambda}^2)^{7/2}} \\
&\exp\left[-\frac{3m_s^2(m_q-m_s)^2\mathbf{k}^2}{(2m_q+m_s)^2(m_q+2m_s)^2(\alpha_{ss\lambda}^2+3\alpha_{ss\rho}^2+4\alpha_{s\lambda}^2)}\right] \times \\
&\left(\mathbf{k}^2(m_q-m_s)^2m_s^2(\alpha_{ss\lambda}+3\alpha_{ss\rho})((m_q+2m_s)\alpha_{ss\lambda}^2-3m_q\alpha_{ss\rho}^2)-(2m_q+m_s)^2(m_q+2m_s)^2 \times \right. \\
&\left.(\alpha_{ss\lambda}^2+3\alpha_{ss\rho}^2+4\alpha_{s\lambda}^2)\left(3(m_q+m_s)\alpha_{ss\lambda}(\alpha_{ss\lambda}-\alpha_{ss\rho})\alpha_{ss\rho}-2(2m_s\alpha_{ss\lambda}+m_q(\alpha_{ss\lambda}-3\alpha_{ss\rho}))\alpha_{s\lambda}^2\right)\right) \\
&/\left(m_qm_s(2m_q+m_s)^2(m_q+2m_s)^2\right). \tag{B8}
\end{aligned}$$

- [1] V. E. Barnes et al. Observation of a Hyperon with Strangeness Minus Three. *Phys. Rev. Lett.*, 12:204–206, 1964.
- [2] Bernard Aubert et al. Measurement of the spin of the Omega- hyperon at BABAR. *Phys. Rev. Lett.*, 97:112001, 2006.
- [3] S. Navas et al. Review of particle physics. *Phys. Rev. D*, 110(3):030001, 2024.
- [4] Medina Ablikim et al. Measurements of the absolute branching fractions of Ω - decays and test of the $\Delta I=1/2$ rule. *Phys. Rev. D*, 108(9):L091101, 2023.
- [5] Medina Ablikim et al. Model-Independent Determination of the Spin of the Ω^- and Its Polarization Alignment in $\psi(3686) \rightarrow \Omega^-\bar{\Omega}^+$. *Phys. Rev. Lett.*, 126(9):092002, 2021.
- [6] Christopher Carone and Howard Georgi. Nonrelativistic chiral expansion and nonleptonic decays of octet and decuplet baryons. *Nucl. Phys. B*, 375:243–262, 1992.
- [7] David A. Egoroff, Ilarion V. Melnikov, and Roxanne P. Springer. Weak nonleptonic Omega- decay in chiral perturbation theory. *Phys. Lett. B*, 451:267–274, 1999.
- [8] Bugra Borasoy and Barry R. Holstein. Resonances in weak nonleptonic Omega- decay. *Phys. Rev. D*, 60:054021, 1999.
- [9] G. Duplancic, H. Pasagic, M. Praszalowicz, and J. Trampetic. Nonleptonic omega- decays and the Skyrme model. *Phys. Rev. D*, 65:054001, 2002.
- [10] H. Galic, D. Tadic, and J. Trampetic. Calculations of Nonleptonic Ω^- Decay Branching Ratios. *Phys. Lett. B*, 89:249–252, 1980.
- [11] Ye Cao, Ming-Xiao Duan, Zhong Tao, and Qiang Zhao. A unified approach for the hadronic weak decays of Λ and $\Sigma^\pm \rightarrow N\pi$. 12 2025.
- [12] Jean-Marc Richard, Qian Wang, and Qiang Zhao. Understanding the shortened lifetime of ${}^3\Lambda$ H. 4 2016.
- [13] Bernard Aubert et al. Measurement of the Spin of the Xi(1530) Resonance. *Phys. Rev. D*, 78:034008, 2008.
- [14] M. Ablikim et al. Study of excited Ξ states in $\psi(3686) \rightarrow K-\Lambda\Xi^-++\text{c.c.}$ *Phys. Rev. D*, 109(7):072008, 2024.
- [15] Li-Ye Xiao and Xian-Hui Zhong. Ξ baryon strong decays in a chiral quark model. *Phys. Rev. D*, 87(9):094002, 2013.
- [16] Muslema Pervin and Winston Roberts. Strangeness -2 and -3 baryons in a constituent quark model. *Phys. Rev.*

C, 77:025202, 2008.

[17] Xian-hui Zhong and Qiang Zhao. Strong decays of heavy-light mesons in a chiral quark model. *Phys. Rev. D*, 78:014029, 2008.

[18] Ru-Hui Ni, Jia-Jun Wu, and Xian-Hui Zhong. Unified unquenched quark model for heavy-light mesons with chiral dynamics. *Phys. Rev. D*, 109(11):116006, 2024.

[19] Ye Cao, Yin Cheng, and Qiang Zhao. Resolving the polarization puzzles in D0 \rightarrow VV. *Phys. Rev. D*, 109(7):073002, 2024.

[20] Jun Wang and Qiang Zhao. Combined analysis of the singly-Cabbibo-suppressed decays of $D^0 \rightarrow VP$. 1 2026.

[21] Peng-Yu Niu, Jean-Marc Richard, Qian Wang, and Qiang Zhao. Hadronic weak decays of Λ_c in the quark model. *Phys. Rev. D*, 102(7):073005, 2020.

[22] Peng-Yu Niu, Jean-Marc Richard, Qian Wang, and Qiang Zhao. Hyperon Weak Radiative Decay. *Chin. Phys. C*, 45(1):013101, 2021.

[23] E. Eichten, K. Gottfried, T. Kinoshita, K. D. Lane, and Tung-Mow Yan. Charmonium: The Model. *Phys. Rev. D*, 17:3090, 1978. [Erratum: Phys.Rev.D 21, 313 (1980)].

[24] Simon Capstick and Nathan Isgur. Baryons in a relativized quark model with chromodynamics. *Phys. Rev. D*, 34(9):2809–2835, 1986.

[25] S. Godfrey and Nathan Isgur. Mesons in a Relativized Quark Model with Chromodynamics. *Phys. Rev. D*, 32:189–231, 1985.

[26] Hui-Hua Zhong, Ming-Sheng Liu, Ru-Hui Ni, Mu-Yang Chen, Xian-Hui Zhong, and Qiang Zhao. Unified study of nucleon and Δ baryon spectra and their strong decays with chiral dynamics. *Phys. Rev. D*, 110(11):116034, 2024.

[27] E. Hiyama, Y. Kino, and M. Kamimura. Gaussian expansion method for few-body systems. *Prog. Part. Nucl. Phys.*, 51:223–307, 2003.

[28] Ming-Sheng Liu, Kai-Lei Wang, Qi-Fang Lü, and Xian-Hui Zhong. Ω baryon spectrum and their decays in a constituent quark model. *Phys. Rev. D*, 101(1):016002, 2020.

[29] Chandni Menapara and Ajay Kumar Rai. Spectroscopic investigation of light strange S=1 Λ , Σ and S=-2 Ξ baryons. *Chin. Phys. C*, 45(6):063108, 2021.

[30] R. N. Faustov and V. O. Galkin. Strange baryon spectroscopy in the relativistic quark model. *Phys. Rev. D*, 92(5):054005, 2015.

[31] Ulrich Loring, Bernard C. Metsch, and Herbert R. Petry. The Light baryon spectrum in a relativistic quark model with instanton induced quark forces: The Strange baryon spectrum. *Eur. Phys. J. A*, 10:447–486, 2001.

[32] R. Bijker, F. Iachello, and A. Leviatan. Algebraic models of hadron structure. 2. Strange baryons. *Annals Phys.*, 284:89–133, 2000.

[33] Yongseok Oh. Xi and Omega baryons in the Skyrme model. *Phys. Rev. D*, 75:074002, 2007.

[34] Yan Chen and Bo-Qiang Ma. Light flavor baryon spectrum with higher order hyperfine interactions. *Nucl. Phys. A*, 831:1–21, 2009.

[35] Georg P. Engel, C. B. Lang, Daniel Mohler, and Andreas Schäfer. QCD with Two Light Dynamical Chirally Improved Quarks: Baryons. *Phys. Rev. D*, 87(7):074504, 2013.

[36] G. Janssen, K. Holinde, and J. Speth. pi rho correlations in the N N potential. *Phys. Rev. C*, 54:2218–2234, 1996.

[37] T. A. Rijken, V. G. J. Stoks, and Y. Yamamoto. Soft core hyperon - nucleon potentials. *Phys. Rev. C*, 59:21–40, 1999.

[38] R. Machleidt, K. Holinde, and C. Elster. The Bonn Meson Exchange Model for the Nucleon Nucleon Interaction. *Phys. Rept.*, 149:1–89, 1987.

[39] A. Pais. Dynamical Symmetry in Particle Physics. *Rev. Mod. Phys.*, 38(2):215–255, 1966.

[40] B. Sakita and K. C. Wali. Relativistic formulation of the SU(6) symmetry scheme. *Phys. Rev.*, 139:B1355–B1367, 1965.

[41] Yin Cheng and Qiang Zhao. Hadronic loop effects on the radiative decays of the first radial excitations of η and η' . *Phys. Rev. D*, 105(7):076023, 2022.

[42] Ye Cao and Qiang Zhao. Study of weak radiative decays of D0 \rightarrow V γ . *Phys. Rev. D*, 109(9):093005, 2024.

[43] Richard Kokoski and Nathan Isgur. Meson Decays by Flux Tube Breaking. *Phys. Rev. D*, 35:907, 1987.

[44] Elizabeth Ellen Jenkins. Hyperon nonleptonic decays in chiral perturbation theory. *Nucl. Phys. B*, 375:561–581, 1992.

[45] J. J. de Swart. The Octet model and its Clebsch-Gordan coefficients. *Rev. Mod. Phys.*, 35:916–939, 1963. [Erratum: Rev.Mod.Phys. 37, 326–326 (1965)].